



Axonal ER Ca²⁺ Release Selectively Enhances Activity-Independent Glutamate Release in a Huntington Disease Model

James P. Mackay,¹ Amy I. Smith-Dijak,^{1,2} Ellen T. Koch,^{1,2} Peng Zhang,^{1,5} Evan Fung,¹ Wissam B. Nassrallah,^{1,3} Caodu Buren,^{1,2} Mandi Schmidt,^{2,4}  Michael R. Hayden,⁴ and  Lynn A. Raymond¹

¹Department of Psychiatry, Djavad Mowafaghian Centre for Brain Health, ²Graduate Program in Neuroscience, ³MD/PhD Program, ⁴Centre for Molecular Medicine and Therapeutics, British Columbia Children's Hospital Research Institute, University of British Columbia, Vancouver, British Columbia V6T 1Z3, Canada, and ⁵Department of Neurosciences, School of Medicine, Case Western Reserve University, Cleveland, Ohio 44106

Action potential (AP)-independent (miniature) neurotransmission occurs at all chemical synapses but remains poorly understood, particularly in pathologic contexts. Axonal endoplasmic reticulum (ER) Ca²⁺ stores are thought to influence miniature neurotransmission, and aberrant ER Ca²⁺ handling is implicated in progression of Huntington disease (HD). Here, we report elevated mEPSC frequencies in recordings from YAC128 mouse (HD-model) neurons (from cortical cultures and striatum-containing brain slices, both from male and female animals). Pharmacological experiments suggest that this is mediated indirectly by enhanced tonic ER Ca²⁺ release. Calcium imaging, using an axon-localized sensor, revealed slow AP-independent ER Ca²⁺ release waves in both YAC128 and WT cultures. These Ca²⁺ waves occurred at similar frequencies in both genotypes but spread less extensively and were of lower amplitude in YAC128 axons, consistent with axonal ER Ca²⁺ store depletion. Surprisingly, basal cytosolic Ca²⁺ levels were lower in YAC128 boutons and YAC128 mEPSCs were less sensitive to intracellular Ca²⁺ chelation. Together, these data suggest that elevated miniature glutamate release in YAC128 cultures is associated with axonal ER Ca²⁺ depletion but not directly mediated by ER Ca²⁺ release into the cytoplasm. In contrast to increased mEPSC frequencies, cultured YAC128 cortical neurons showed less frequent AP-dependent (spontaneous) Ca²⁺ events in soma and axons, although evoked glutamate release detected by an intensity-based glutamate-sensing fluorescence reporter in brain slices was similar between genotypes. Our results indicate that axonal ER dysfunction selectively elevates miniature glutamate release from cortical terminals in HD. This, together with reduced spontaneous cortical neuron firing, may cause a shift from activity-dependent to -independent glutamate release in HD, with potential implications for fidelity and plasticity of cortical excitatory signaling.

Key words: axons; calcium; endoplasmic reticulum; Huntington disease; miniature neurotransmission; patch clamp

Significance Statement

Miniature neurotransmitter release persists at all chemical neuronal synapses in the absence of action potential firing but remains poorly understood, particularly in disease states. We show enhanced miniature glutamate release from cortical neurons in the YAC128 mouse Huntington disease model. This effect is mediated by axonal ER Ca²⁺ store depletion, but is not obviously due to elevated ER-to-cytosol Ca²⁺ release. Conversely, YAC128 cortical pyramidal neurons fired fewer action potentials and evoked cortical glutamate release was similar between WT and YAC128 preparations, indicating axonal ER depletion selectively enhances miniature glutamate release in YAC128 mice. These results extend our understanding of action potential independent neurotransmission and highlight a potential involvement of elevated miniature glutamate release in Huntington disease pathology.

Received Aug. 19, 2022; revised Mar. 8, 2023; accepted Mar. 15, 2023.

Author contributions: J.P.M., E.T.K., and L.A.R. designed research; J.P.M., A.I.S.-D., E.T.K., E.F., W.B.N., C.B., and M.S. performed research; J.P.M., E.T.K., E.F., and W.B.N. analyzed data; J.P.M. wrote the first draft of the paper; J.P.M., A.I.S.-D., E.T.K., P.Z., E.F., W.B.N., C.B., M.S., M.R.H., and L.A.R. edited the paper; J.P.M. wrote the paper; P.Z. and M.R.H. contributed unpublished reagents/analytic tools.

This work was supported by resources made available through the Dynamic Brain Circuits cluster, the DataBinge forum, and the NeuroImaging and NeuroComputation Center at the University of British Columbia (UBC) Djavad Mowafaghian Center for Brain Health (RRID:SCR_019086); and Canadian Institutes of Health Research (CIHR) Foundation Grants FDN-143210 to L.A.R. and FDN-154278 to M.R.H. and Project Grant PJT-178043 to L.A.R. J.P.M. was supported by a Michael Smith Foundation for Health Research Trainee Award RT-2020-0614 and a Hereditary Disease Foundation Fellowship. C.B. was supported by a University of British Columbia 4-year Graduate Fellowship (UBC 4-YF). A.I.S.-D. was supported by a CIHR Canada Graduate

Scholarship Doctoral award and a UBC 4-YF. E.T.K. was supported by a CIHR Canada Graduate Scholarship Master's award, Canadian Open Neuroscience Platform Scholar award, and UBC 4-YF. M.S. was supported by a Vanier Canada Graduate Scholarship and a UBC 4-YF. W.B.N. was supported by a UBC-CHIR-MD/PhD studentship and a Vanier Canada Graduate Scholarship. L.A.R. holds the UBC Department of Psychiatry Louise A. Brown Chair in Neuroscience. M.R.H. holds a Canada Research Chair. We thank Dr. Anne Marie Craig (UBC) for expert advice on experiments using rSyph-GCaMP6m; Pankaj Kumar Gupta for providing data analysis code; and Dr. Lily Zhang and Dr. Rujun Kang for technical support and assistance.

The authors declare no competing financial interests.

Correspondence should be addressed to Lynn A. Raymond at Lynn.raymond@ubc.ca.

<https://doi.org/10.1523/JNEUROSCI.1593-22.2023>

Copyright © 2023 the authors

Introduction

Neurotransmitter release occurs independently of Na⁺-driven action potentials (APs) at most, if not all, neuronal synapses. This activity-independent (or “miniature”) release has been shown to be physiologically relevant and can serve distinct biological roles. Dendritic protein synthesis, network excitability, and neurodevelopment are among the processes influenced by miniature transmission (Carter and Regehr, 2002; Sharma and Vijayaraghavan, 2003; Sutton et al., 2006; Andreae and Burrone, 2015). In addition, recent studies suggest that enhanced miniature glutamate release can drive pathologic conditions, contributing to major depressive disorder and neurodegeneration (Fishbein and Segal, 2007; Chanaday et al., 2021).

In contrast to activity-dependent release, several studies report that miniature synaptic events persist in the absence of extracellular Ca²⁺ (Yamasaki et al., 2006; Xu et al., 2009); however, such events still appear to be largely Ca²⁺-dependent, based on their near complete blockade by the fast, membrane-permeable Ca²⁺ chelator BAPTA-AM in cortical cultures (Xu et al., 2009). Rather, Ca²⁺ originating from axonal ER Ca²⁺ stores appears to largely mediate this type of miniature release (Emptage et al., 2001). However, other studies report a direct dependence of miniature release on extracellular Ca²⁺, mediated by stochastic openings of voltage-gated Ca²⁺ channels (VGCCs) (Ermolyuk et al., 2013), or ER Ca²⁺ depletion and consequent Ca²⁺ entry via the store-operated Ca²⁺ channel (SOC) response (Chanaday et al., 2021). One study also reported miniature release in cortical cultures was mediated by the calcium sensing receptor (CaSR), a GPCR expressed on the plasma membrane of cortical terminals (Vyleta and Smith, 2011), which when activated by extracellular Ca²⁺ (or other agonists), increased miniature event frequencies independently of intracellular Ca²⁺. Although these studies suggest a complex, diverse regulation of AP-independent neurotransmission, there is general consensus that most mini events require Ca²⁺ (extracellular or intracellular). Moreover, involvement of presynaptic ER Ca²⁺ is a recurrent theme, with ER stores either providing Ca²⁺ for vesicular release directly or recruiting SOC entry.

Abnormalities in neuronal Ca²⁺ handling, particularly in relation to ER function (Tang et al., 2009), are key features of multiple age-related neurodegenerative disorders, including Huntington disease (HD) (Raymond, 2017), a fatal, autosomal dominantly-inherited neurodegenerative disorder caused by a polyglutamine-encoding CAG repeat-expansion (>35 repeats) in exon 1 of the huntingtin gene (Huntington’s Disease Collaborative Research Group, 1993). Abnormal glutamate signaling is also a key HD feature and likely contributes to synaptic dysfunction and the relatively selective degeneration of GABAergic striatal spiny projection neurons (SPNs) and cortical pyramidal neurons (CPNs) in HD (Graveland et al., 1985; Vonsattel et al., 1985; Beal et al., 1986; Hantraye et al., 1990; Raymond, 2017; Cepeda and Levine, 2022). Increased postsynaptic extrasynaptic NMDAR expression (Zeron et al., 2002; Fan et al., 2007; Milnerwood et al., 2010; Botelho et al., 2014; Plotkin et al., 2014; Kovalenko et al., 2018), which triggers cell death signaling (Hardingham and Bading, 2010), is thought to contribute to HD pathology. Altered glutamate release from cortical projections onto SPNs has also been reported in multiple HD mouse models (Cepeda et al., 2003; Joshi et al., 2009; Raymond et al., 2011), but the direction of this effect appears to be model and disease-stage dependent (Joshi et al., 2009).

The ER’s apparent involvement in regulating miniature glutamate release suggests a link between ER dysfunction and altered glutamate signaling in HD. Mutant huntingtin protein directly

interacts with ER Type 1 inositol (1,4,5)-triphosphate receptors (IP3Rs), sensitizing their Ca²⁺ release in response to IP3 (Tang et al., 2003). In addition, ryanodine receptors (RyRs: ER-localized Ca²⁺ channels that mediate Ca²⁺-induced Ca²⁺ release) are constitutively leaky in HD mouse models (Suzuki et al., 2012). Mutant huntingtin is expressed at presynaptic terminals (Li et al., 2003); however, ER Ca²⁺ handling in this subcellular compartment has not been studied in HD. Here, we investigate presynaptic Ca²⁺ signaling and miniature glutamate release in cortical pyramidal neurons from premanifest HD-model mice.

Materials and Methods

Culture preparation. All animal-related procedures were approved by and adhered to the guidelines of the University of British Columbia Committee on Animal Care and the Canadian Council on Animal Care (protocols A17-0295, A15-0069, and A19-0076). Cultures were prepared from both male and female embryonic day 17–18 pups from either WT FVB/N or transgenic yeast artificial chromosome-containing mice expressing the full-length human huntingtin genomic DNA with 128 CAG repeats (YAC128). YAC128 mice were maintained on the FVB/N background (homozygous line 55). WT and YAC128 mice used for *ex vivo* slice experiments (below) and bred for culture preparation (above) were group-housed under controlled conditions, free of known pathogens, at room temperature (22°C–24°C), under a 12 h light/dark cycle. Cortical cultures used in patch-clamp electrophysiology, and Ca²⁺-imaging experiments were prepared as previously described (Milnerwood et al., 2012; Smith-Dijk et al., 2019) and plated at a density of 225,000 neurons/ml. In a subset of experiments, a portion of the total 2.7 million cortical neurons (plated per 24-well culture) were transfected with one or more transgenic reporters including the following: GFP (Addgene plasmid 37825); a synaptophysin-tagged GCaMP6-M construct (a generous gift from Anne Marie Craig, University of British Columbia); JGCaMP7-F (Addgene plasmid 104489); a postsynaptic density 95 (PSD95)-tagged M-cherry construct; or a GFP-tagged internally expressed anti-PSD95 antibody (a generous gift from D.B. Arnold, University of Southern California) (Gross et al., 2013).

Electrophysiology. An Axopatch 200B amplifier and pClamp 9.2 software (Molecular Devices) were used to acquire whole-cell patch-clamp electrophysiology recordings. Data were digitized at 20 kHz and low-pass filtered at 1 kHz. For electrophysiology experiments, cultures were perfused with extracellular fluid (ECF) containing the following (in mM): 167 NaCl, 2.4 KCl, 10 glucose, 10 HEPES, 2 CaCl₂, and 1 MgCl₂; NaOH (1 mM) was used to adjust the pH to 7.30, and the osmolarity was adjusted to 305–310 mOsm. TTX (500 nM) and picrotoxin (PTX) (50 mM) were added to this ECF to block sodium channel-mediated APs and GABA_A receptor-mediated currents, respectively. Neurons were patched with borosilicate glass pipettes pulled to a tip resistance of 3–6 MΩ when back-filled with intracellular solution containing the following (in mM): 130 Cs-methanesulfonate, 5 CsCl, 4 NaCl, 1 MgCl, 10 HEPES, 5 EGTA, 5 QX-314 Cl, 0.5 Na-GTP, 10 Na-phosphocreatine, and 5 Mg-ATP (~286 mOsm). During experiments, neurons were held at –70 mV in voltage-clamp, with hyperpolarizing voltage steps (–10 mV) performed periodically to measure intrinsic membrane properties. Under these conditions, AMPAR-mediated mEPSCs appeared as transient inward current deflections. Recordings with a series resistance >25 MΩ were excluded from analysis; typical values were between 15 and 20 MΩ. A minimum of 2 min following establishment of the whole-cell configuration was allowed before experimental measurements, so neurons could fully dialyze with intracellular solution and membrane resistance and holding current stabilize. For experiments involving within-cell drug applications, a maximum 20% change in series resistance between control and drug measurements was tolerated. In these cases, drugs were applied locally to neurons with a fast perfusion system. Mini Analysis software (Synaptosoft) was used to detect mEPSCs and extract relevant parameters. A minimum of 100 and no more than 1000 mEPSCs were analyzed per neuron per experimental condition.

CPN morphology. CPNs in WT and YAC128 cultures were labeled by transfecting a subset of neurons (1 of 2.7 million) with a cytoplasmic GFP at the time of plating. Cultures were subsequently fixed at DIV17–19 and GFP-labeled CPN dendritic arbors imaged on a Zeiss Axiovert 200M fluorescence microscope (20× magnification, 0.8 NA), with a Zeiss 702 monochrome camera, using Zen software. Multiple image Z stacks were acquired and X,Y-tiling was used to ensure entire dendritic arbors were visualized. Images were exported to Fiji-ImageJ for analysis by a blinded observer. Images were flattened using the maximum Z-projection function. Background subtraction was performed, and neuronal processes were thresholded following adjustment of brightness and contrast. Automated Sholl analysis was performed using the ImageJ Sholl analysis plugin.

Excitatory cortical synapse staining. A subset of neurons (2 of 2.7 million) in WT and YAC128 cortical cultures were transfected with a GFP-tagged internally-expressed anti-PSD95 antibody (intrabody) (Gross et al., 2013) at the time of plating. At DIV17–DIV19, cells were fixed and stained for VGlut1 and the GluA2 AMPAR subunit as previously described (Buren et al., 2016). Briefly, cultures were first live-stained with a primary mouse anti-GluA2 antibody (Millipore), then fixed and stained with a secondary AlexaFluor-568-conjugated donkey anti-mouse antibody (Invitrogen). Subsequently, cultures were incubated with a primary guinea pig anti-VGlut1 antibody (Millipore), then stained with a secondary AMCA-conjugated donkey anti-guinea pig antibody (Jackson ImmunoResearch Laboratories). To amplify the GFP fluorescence of the anti-PSD95 intrabody, cultures were also incubated with a primary chicken anti-GFP antibody (1:1000) (Millipore), followed by a secondary AlexaFluor-488-conjugated antibody (1:500) (Invitrogen). Cultures were imaged on a Zeiss Axiovert 200M fluorescence microscope (63× magnification, 1.4 NA), using a Zeiss 702 monochrome camera and Zen software. CPNs expressing the anti-PSD95 intrabody were identified based on their diffuse cytoplasmic GFP fill, with bright GFP-labeled puncta expressed at dendritic spines. A portion of each CPN's arbor, containing multiple secondary and tertiary dendrites, was selected for imaging and sufficient image Z stacks were acquired to adequately capture all dendritic processes present in a given 63× field. Images were exported to Fiji-ImageJ for analysis by a blinded observer and flattened using the maximum Z-projection function. For each CPN image, the GFP channel was used to identify three secondary or tertiary dendritic segments, at least 40 μm away from the CPN soma, over which ROIs were drawn. Following background subtraction, fluorescent puncta in the green (GFP), red (AlexaFluor-568), and blue (AMCA) channels, visible within dendritic ROIs, were manually thresholded and detected with the analyze particles function. The ImageJ colocalization plugin was used to identify triple-colocalized puncta (PSD95, GluA2, and VGlut1), which we interpreted as functional CPN glutamatergic synapses. Synapse density was defined as the number of triple-colocalized puncta present within a dendritic segment divided by the area of the segment and averaged across all three dendrites analyzed in a given CPN.

GCaMP imaging. To directly image cytosolic Ca²⁺ in axonal boutons of neurons in our cortical monocultures, we transfected 1 million cells (of a total 2.7 million) at time of plating with a rat synaptophysin-tagged GCaMP6-M construct (rSyph-GCaMP6m). The rSyph-GCaMP6m construct was created by fusing GCaMP6-M (Chen et al., 2013) with the full-length rat synaptophysin protein (1–307 amino acids) via a small glycine-serine linker and inserting the fused rSyph-GCaMP6-M construct into a pLL3.7-hSyn vector to achieve neuron-selective expression. For some experiments, the same 1 million cells were also transfected at time of plating with an M-cherry-tagged PSD95 construct; in these cases, presumptive glutamatergic terminals targeting other CPNs were identified as rSyph-GCaMP6m-expressing boutons colocalized with M-Cherry-labeled postsynaptic spines. In other experiments, 1 million of the total 2.7 million cortical neurons were transfected at the time of plating with jGCaMP7-F to monitor AP-dependent somatic Ca²⁺ events.

For all Ca²⁺-imaging experiments, cultures were plated on 8-well cover glass chambers (Fisher Scientific, Nunc, Lab-Tek) and imaged at DIV17–DIV19 with a Zeiss Axiovert 200M fluorescence microscope (63× magnification, 1.4 NA), using a Zeiss 702 monochrome camera and Zen software. Movies were acquired using the Zen time-series

mode. For experiments where only Ca²⁺-dependent GCaMP fluorescence was measured, data were acquired at 10 Hz (100 ms exposure per frame), with camera-steaming enabled. In some experiments, we simultaneously monitored Ca²⁺-dependent and independent (isosbestic) GCaMP fluorescence in boutons by rapidly switching between two filter cubes: one with a 488 nm excitation filter (Ca²⁺-dependent) and the other with a 405 nm (isosbestic) excitation filter (both filter cubes used 525 nm emission filters). In these experiments, a 100 ms exposure time was used for both channels, and data were acquired at 0.6 Hz per channel. These experiments were performed in standard ECF (as above) with or without TTX (500 nM) present, but in the absence of PTX.

Spontaneous Ca²⁺ waves were commonly evident in rSyph-GCaMP6m-labeled axons, particularly when AP-dependent Ca²⁺ events were blocked with TTX. These signals were quantified either with the Astrocyte Quantitative Analysis (AQuA) software (running in MATLAB) (Wang et al., 2019) or an in house software developed to export and quantify GCaMP time courses from boutons colocalized with MCherry-labeled dendritic spines (also in MATLAB). Rather than relying on neuronal morphology-based segmentation, AQuA defines events as spatially and temporally connected signals surpassing user-defined thresholds. This allowed the spatial extent of Ca²⁺ waves to be quantified, but also meant that multiple boutons were often classified as part of a single event when contacted by a given Ca²⁺ wave. Frequencies of AQuA-detected spontaneous axonal events were quantified as numbers of events occurring within a standardized area [178.6 μm × 113.1 μm (a maximal 63× FOV)], during a standardized (3 min) consecutive imaging interval. AQuA detection parameters were empirically determined to best match a small number of manually analyzed experiments and applied across all cultures and conditions analyzed to facilitate meaningful comparisons.

Our in-house software adapted an algorithm from Nelson et al. (2015) to detect centroids of fluorescent puncta and to identify colocalizations between puncta in separate imaged channels (here GCaMP and MCherry-PSD95) based on a user-defined minimum distance between centroids (Nelson et al., 2015). GCaMP puncta (presumptive boutons) were classified as colocalized with CPN dendritic spines when their centroids fell within 4 pixels of an MCherry-labeled particle centroid. Both Ca²⁺-dependent and isosbestic GCaMP fluorescence was measured in these experiments (as above). As background autofluorescence was often high in the isosbestic channel, we restricted analysis of GCaMP puncta to those in which signal/noise was sufficient for our algorithm to detect corresponding puncta in the isosbestic channel. Each point of a bouton's Ca²⁺-dependent GCaMP time course was divided by the corresponding Ca²⁺-independent isosbestic channel signal to account for differences in GCaMP expression between individual boutons and cultures and facilitate quantitative Ca²⁺ comparisons. To compare relative resting bouton cytosolic Ca²⁺ levels between genotypes and various pharmacological conditions, we quantified both mean and minimum (488/405) fluorescence values of individual bouton traces (following low pass filtering to remove miniature Ca²⁺ events). The MATLAB FindPeaks function was used to detect miniature events in these (488/405) fluorescence traces and extract relevant parameters, including peak event amplitudes and event half-amplitude widths. Event frequencies were calculated by dividing numbers of detected miniature events in a trace by the trace interval in minutes.

In a subset of experiments conducted in the presence of TTX, responses of individual WT or YAC128 rSyph-GCaMP6m-labeled synaptic boutons to caffeine or ionomycin were measured. In these experiments, culture fields were imaged for 3 min (as above), after which caffeine (1 mM) or ionomycin (10 μM) was applied and imaging continued for an additional 1–2 min. For these experiments, an analyzer (blinded to culture genotype) used Fiji-ImageJ (National Institutes of Health) to manually assign elliptical ROIs to 10 boutons per movie and exported each ROI's fluorescence-intensity time course. Time courses were subsequently imported to MATLAB, where the curve fitting tool was used to model each time course's photobleaching profile based on the initial 3 min recording; this curve was then extrapolated to the entire time course including caffeine treatment. The resultant "bleaching curve" was subtracted from the raw rSyph-GCaMP6m fluorescence curve and this time course subsequently divided by the "bleaching curve" to yield a final curve

reflecting the caffeine response in DF/F units. Ionomycin experiments were analyzed similarly, except in this case, the blinded analyzer selected 10 active boutons (showing at least 1 clear Ca²⁺ event during the initial 3 min recording) and 10 inactive boutons (with no Ca²⁺ events present during the initial 3 min recording). Time courses derived from inactive boutons were exported to MATLAB, where the ionomycin-mediated DF/F responses were calculated as above. In the case of active boutons, spontaneous events occurring during the first 3 min were detected with MATLAB's FindPeaks function and excised from the raw fluorescence time courses before curve fitting, but otherwise processed as above.

As expected, spontaneous events were far more frequent when rSynp-GCaMP6m-expressing cultures were imaged in the absence of TTX. Most boutons showed many events during a 3 min imaging session. These events, which were presumably driven by the AP-dependent opening of VGCCs, were far shorter in duration than typical TTX-resistant events. To assess for genotype differences in these signals, a blinded analyzer used Fiji-ImageJ to randomly assign elliptical ROIs to 20 boutons per movie and exported each ROI's fluorescence-intensity time course to MATLAB. The high frequency of AP-dependent events often precluded extracting the photobleaching profile of a bouton's time course, necessitating an alternative means of calculating the DF/F values of spontaneous events. We therefore averaged the gray-value fluorescence intensity across an entire time course, subtracted this average fluorescence pointwise from the time course, then divided pointwise by the average fluorescence to convert to DF/F units. Any nonstationary present in these DF/F time-series because of photobleaching was removed with the MATLAB detrend function. The MATLAB FindPeaks function was subsequently used to detect events in these DF/F traces as above. Bouton event frequencies and event parameters in the absence of TTX were compared between WT and YAC128 cultures under baseline conditions and following application of ryanodine (5 μ M). A similar algorithm run entirely in MATLAB was used to monitor activity-dependent somatic Ca²⁺ events in JGCaMP7f expressing cortical neurons.

Intensity-based glutamate-sensing fluorescence reporter (iGluSnFR) imaging in acute brain slices. Expression of the genetically encoded iGluSnFR (Marvin et al., 2013) in WT and YAC128 mice was achieved with stereotaxic injection of a viral construct as described previously (Parsons et al., 2016). Briefly, under isoflurane anesthesia, 1–1.4 μ l of the AAV1.hSyn.iGluSnFR.WPRE.SV40 construct (Penn Vector Core; Loren Looger, Janelia Farm Research Campus of the Howard Hughes Medical Institute) was directly injected into the dorsal striatum of 4- to 6-week-old mice. Following surgery, mice were closely monitored for a week to ensure adequate recovery.

After waiting 3–6 weeks, to ensure optimal iGluSnFR expression, acute brain slices from 2- to 4-month-old YAC128 mice and age-matched WT controls were prepared as described previously (Parsons et al., 2016; Koch et al., 2018). Briefly, mice were decapitated following deep isoflurane anesthesia, and their brains rapidly removed and placed in an ice-cold slicing solution, bubbled with carbogen (95% O₂, 5% CO₂) gas, containing the following (in mM): 125 NaCl, 2.5 KCl, 25 NaHCO₃, 1.25 NaH₂PO₄, 2.5 MgCl₂, 0.5 CaCl₂, and 10 glucose; 300- μ m-thick striatum-containing sagittal brain slices were cut with a Leica VT1200S vibratome. Slices were subsequently incubated for 30 min in warmed ACSF containing 2 mM CaCl₂ and 1 mM MgCl₂; ACSF constituents and concentrations were otherwise identical to the slicing solution (above).

Slices were transferred to a submerged recording chamber for experiments and perfused with carbogen-bubbled ACSF at a rate of 2–3 ml/min at room temperature. Cortical release of glutamate into the striatum was evoked by delivering paired 0.1 ms electrical pulses at 100 Hz with an A-M Systems isolated pulse stimulator (model 2100) and tungsten monopolar stimulating electrode (tip resistance 0.1 M Ω). The electrode was placed into a corpus callosum segment adjacent to the dorsal striatum at an ~50–100 μ m depth. During and immediately before the electrical stimulation, iGluSnFR fluorescence was excited with a 470 nm LED; slices were not illuminated between experimental measurements to minimize phototoxicity and bleaching. Stimulation and LED activation were triggered by Clampex software (Molecular Devices). iGluSnFR fluorescence was isolated with a 530 nm bandpass filter and imaged with a

CCD camera (1 M60, Pantera, Dalsa) and XCAP software (Epix) at 150 Hz with 8 \times 8 pixel binning. Experimental measurements encompassing four stimulation trials and two blank trials were performed at 3 min intervals. The four stimulation trials were averaged and the blank trials, in which slice fluorescence was imaged without electrical stimulation, were averaged and used to account for photobleaching and to calculate the stimulation mediated changes in iGluSnFR fluorescence over basal fluorescence (Δ F/F) as described previously (Parsons et al., 2016). Videos were analyzed offline with ImageJ software. The average iGluSnFR signal was measured over 10 \times 10 pixel (93.8 \times 93.8 μ m) ROI placed over the maximal area of evoked iGluSnFR activity within the striatum adjacent to the stimulating electrode. To normalize for potential differences in iGluSnFR expression between slices, in subsets of experiments we applied a near saturating dose of glutamate (10 mM) in the presence of TTX (500 nM), kynurenic acid (100 μ M), and DL-TBOA (10 μ M) to slices following evoked iGluSnFR experiments. Evoked iGluSnFR measurements and the subsequent exogenous glutamate calibrations were performed under identical excitation LED intensity. Peak evoked DF/F responses were normalized to the mean iGluSnFR fluorescence grayscale intensity over the analysis ROI following the plateau of this signal in the continued presence of the glutamate calibration solution.

Experimental design and statistical analysis. Statistical analysis and creation of figures were performed using GraphPad Prism (version 7). All data distributions were tested for normality with the D'Agostino-Pearson omnibus normality test.

The Student's unpaired *t* test was used for unpaired comparisons between two data groups, such as when mean mEPSC frequencies were compared between WT and YAC128 neurons, as long both data groups were normally distributed. When one or both groups failed, the D'Agostino-Pearson omnibus normality test, the nonparametric Mann-Whitney test was used instead.

When parameters of the same group of neurons or axonal boutons were compared before and after a drug treatment, statistical significance was assessed with the Student's paired *t* test, unless data points in the control or drug-treatment group failed the D'Agostino-Pearson omnibus normality test, in which case, the nonparametric Wilcoxon matched-pairs signed rank test was used instead.

A two-way ANOVA with the Bonferroni post test (as appropriate) was used when testing for genotype differences in a dependent variable measured at different time points, as was the case for our brain-slice iGluSnFR experiments.

Depending on the experimental design, "*n*" numbers in figures refer to number of neurons, numbers of imaged culture fields, numbers of individual axonal boutons, or numbers of brain slices. Clarifying details are present within individual figure legends, as are the numbers of culture batches or mice used.

Differences in mean values were considered significant at *p* < 0.05. Comprehensive descriptions of statistical analysis are included in the figure legends.

Results

mEPSC frequencies are elevated in YAC128 striatal and cortical neurons at early time points

Our group previously found that mEPSCs were significantly more frequent, compared with WT, in striatal SPNs from yeast artificial chromosome (YAC128) mouse-derived cortical-striatal cocultures at DIV14. This genotype difference was not seen at DIV 21, at which point higher presynaptic miniature glutamate release rates may have been masked by a significant reduction in YAC128 SPN total dendritic length relative to WT (and therefore reduced total excitatory synapse numbers) (Buren et al., 2016).

The above data indicated a higher rate of AP-independent glutamate release from YAC128 presynaptic CPN terminals at early time points. To follow-up on these findings, we capitalized on a relatively simpler culture preparation containing only cortex-derived neurons, along with YAC128 mouse-derived cortical-striatal brain slices, to mechanistically dissect how mutant

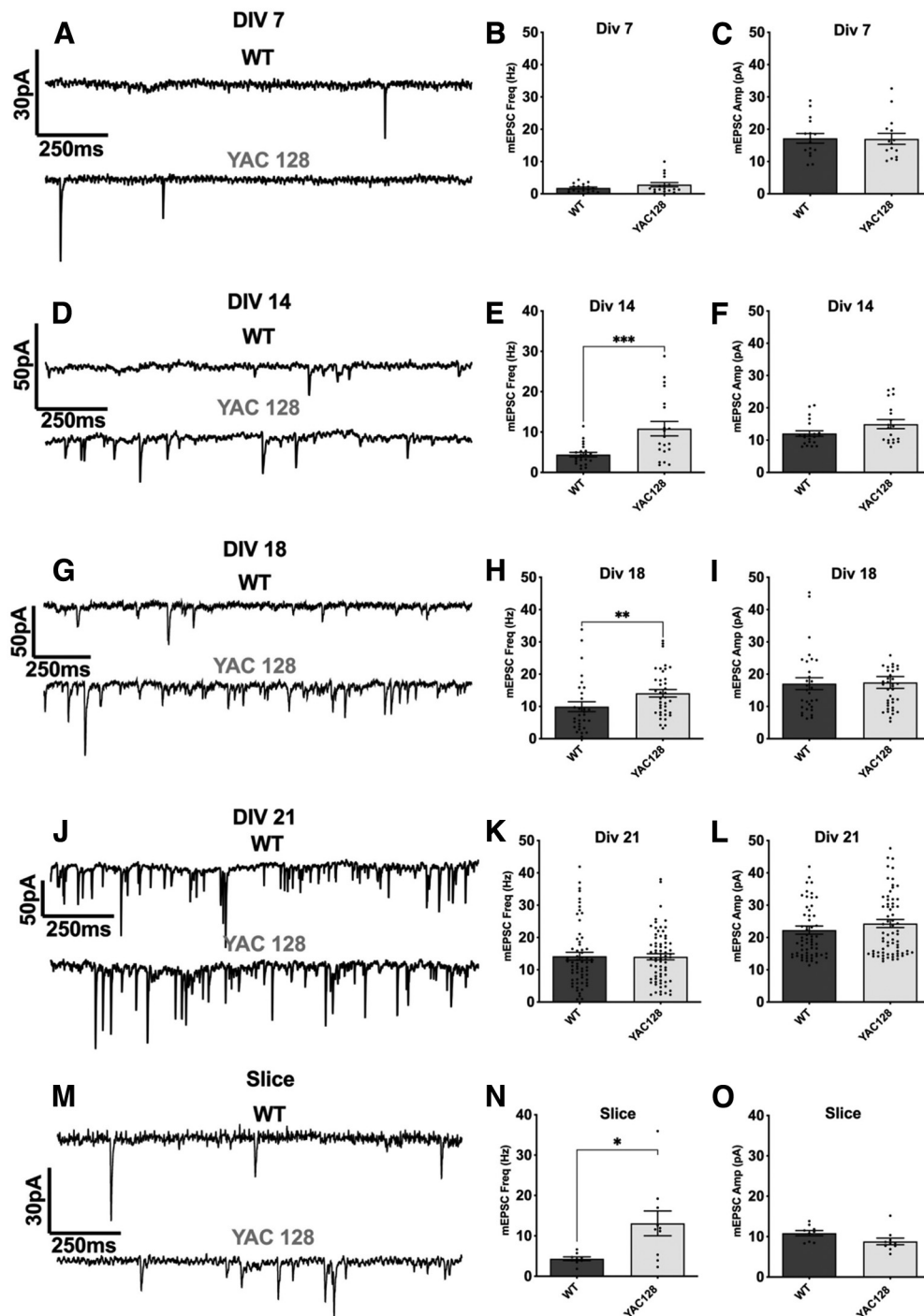


Figure 1. mEPSC frequencies are elevated in YAC128 cortical cultures at early DIV time points and in YAC128 mouse-derived acute brain slices. Representative traces (**A,D,G,J,M**) and population data for mEPSCs (frequency in **B,E,H,K,N**; amplitude in **C,F,I,L,O**) recorded from cultured WT and YAC128 CPNs (**A–L**), or SPNs in acute brain slices from WT and YAC128 mice (**M–O**). All recordings were made in voltage clamp with a holding potential of -70 mV in solution containing TTX (500 nM) and PTX (50 μ M). **A–C**, Recordings made from CPNs in DIV7 cultures. Mean mEPSC frequency (**B**) was 1.8 ± 0.3 Hz ($n = 18$; 3 cultures) in WT CPNs and 2.8 ± 0.7 Hz ($n = 17$; 4 cultures) in YAC CPNs; this difference was not statistically significant [$t_{(33)} = 1.449$; $p = 0.1567$; Student's unpaired t test]. Mean mEPSC amplitudes (**C**) were similar in WT and YAC128 cultures: 17.2 ± 1.5 pA ($n = 18$; 3 cultures) and 17.0 ± 1.7 pA ($n = 17$; 4 cultures), respectively [$t_{(33)} = 0.06936$; $p = 0.9452$; Student's unpaired t test]. **D–F**, Recordings were made from CPNs in DIV14 cortical cultures. Mean mEPSC frequency (**E**) was significantly higher in YAC128 CPNs [10.8 ± 1.8 Hz ($n = 20$; 6 cultures)] compared with WT CPNs [4.4 ± 2.6 Hz ($n = 22$; 4 cultures)] [$t_{(40)} = 3.555$; $p = 0.0010$; Student's unpaired t test]. Mean CPN mEPSC amplitudes (**F**) were not significantly different in WT and YAC128 cultures: 12.1 ± 0.8 pA ($n = 22$; 4 cultures) and 15.0 ± 1.4 pA ($n = 20$; 6 cultures), respectively [$t_{(40)} = 1.807$; $p = 0.0786$; Student's unpaired t test]. **G–I**, Recordings were made from CPNs in DIV18 cortical cultures. Mean CPN mEPSC frequency (**H**) was significantly higher in YAC128 cortical cultures [14.1 ± 1.2 Hz ($n = 38$; 10 cultures)] compared with WT cultures [9.9 ± 1.5 Hz ($n = 30$; 15 cultures)] [$p < 0.0059$ (exact); Mann–Whitney test]. Mean CPN mEPSC amplitudes (**I**) were similar in WT and YAC128 cultures: 17.0 ± 1.8 pA ($n = 30$; 15 cultures) and 17.4 ± 1.8 pA ($n = 38$; 10 cultures), respectively [$p = 0.8643$ (exact); Mann–Whitney test]. **J–L**, Recordings were made from CPNs in DIV21 cortical cultures. Mean CPN mEPSC frequency (**K**) was similar in WT and YAC128 cultures: 14.2 ± 1.2 Hz ($n = 62$; 17 cultures) and 14.0 ± 0.9 Hz ($n = 71$; 23 cultures), respectively [$p = 0.5626$ (exact); Mann–Whitney test]. Mean CPN mEPSC amplitudes (**L**) were similar in WT and YAC128 cultures: 22.3 ± 1.3 pA ($n = 62$; 17 cultures) and 24.3 ± 1.2 pA ($n = 71$; 23 cultures), respectively [$p = 0.2143$ (exact); Mann–Whitney test]. **M–O**, Recordings were made from SPNs in acute striatum-containing brain slices from 2- to 4-month-old WT and YAC128 mice. Mean SPN mEPSC frequency (**N**) was significantly higher in YAC128 SPNs [13.1 ± 3.1 Hz ($n = 10$; 5 mice)] compared with WT cultures [4.3 ± 0.5 Hz ($n = 9$; 4 mice)] [$t_{(17)} = 2.683$; $p = 0.00157$; Student's unpaired t test]. Mean SPN mEPSC amplitudes (**O**) were not significantly different in WT and YAC128 slices: 10.8 ± 2.0 pA ($n = 9$; 4 mice) and 8.8 ± 2.6 pA ($n = 10$; 5 mice), respectively [$t_{(17)} = 1.922$; $p = 0.0716$; Student's unpaired t test]. * $p < 0.05$. ** $p < 0.01$. *** $p < 0.001$.

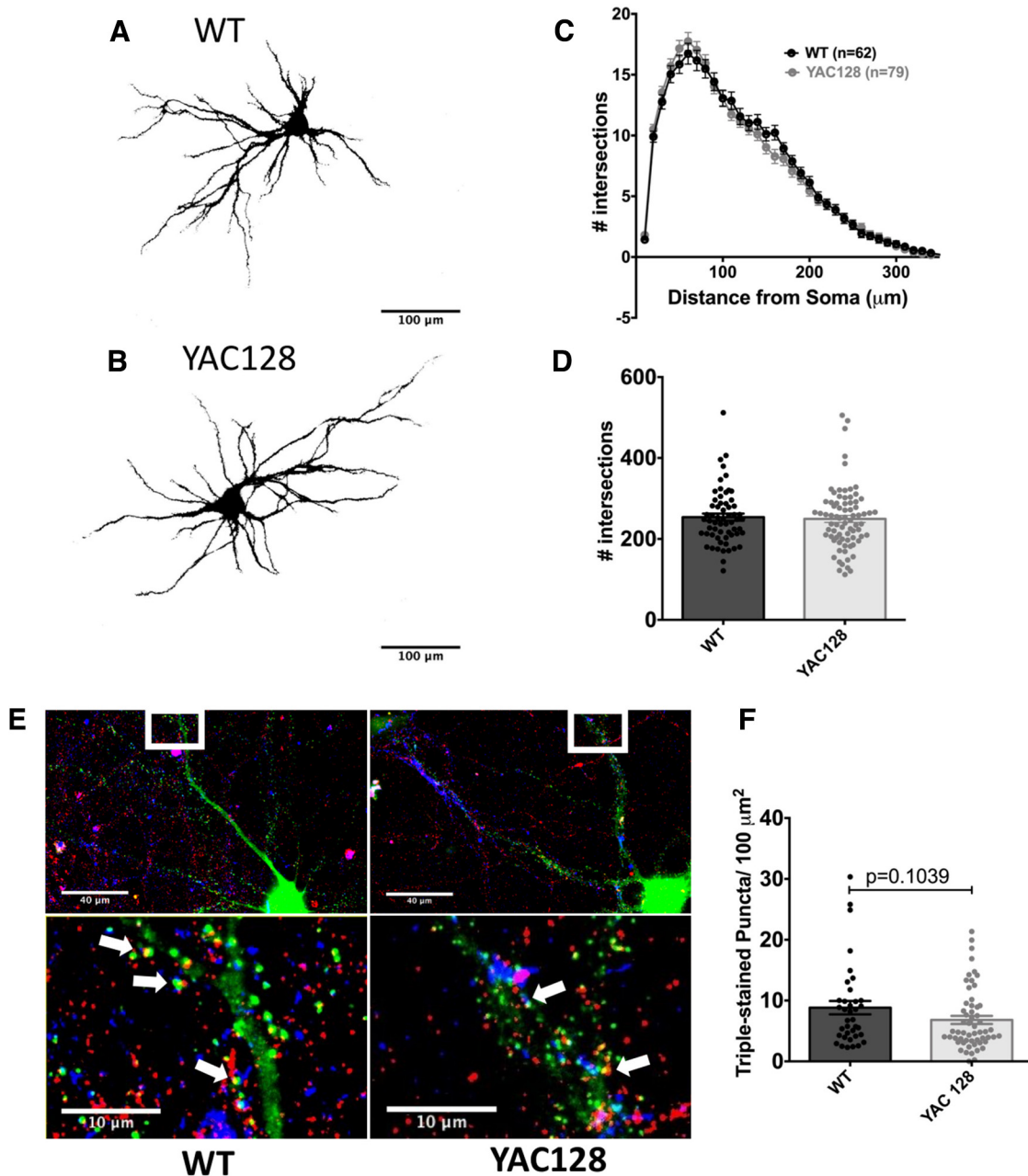


Figure 2. Dendritic complexity and excitatory synapse numbers are similar in WT and YAC128 cortical cultures. **A, B**, Representative images generated by thresholding a merged Z stack of a GFP-expressing WT CPN (**A**) and YAC128 CPN (**B**). **C**, Number of dendritic intersections through concentric Sholl circles centered on the soma of GFP-filled WT and YAC128 CPNs of radii between 10 and 450 μm . WT and YAC128 CPNs have nearly identical dendritic branching distributions [two-way ANOVA; genotype: $F_{(1, 6165)} = 1.168, p < 0.2799$; distance from soma: $F_{(44, 6165)} = 381.6, p < 0.0001$; interaction: $F_{(44, 6165)} = 0.9868, p < 0.4966$]. **D**, Total numbers of Sholl intersections, which reflect general neuronal complexity, were similar in WT and YAC128 CPNs: 254.0 ± 8.8 ($n = 61$; 4 cultures) and 249.5 ± 8.7 ($n = 78$; 4 cultures), respectively [$p = 0.7263$ (exact); Mann–Whitney test]. **E**, Representative merged Z stack from a WT CPN (left panels) and YAC128 CPN (right panels) with merged green, red, and blue channels showing staining of a genetically encoded internally expressed GFP-tagged anti-PSD95 antibody (green), anti-AMPA GluA2 subunit immuno-staining (red), and anti-VGLUT1 immuno-staining (blue), respectively. Bottom, Expanded view of a segment of dendrite with arrows pointing to a subset of colocalized PSD95, GluA2, and VGLUT1 puncta, which were counted as presumed functional synapses. For illustrative purposes, the brightness and contrast of the individual channels were adjusted to best illustrate the punctate fluorescence. **F**, Numbers of presumed functional synapses (identified as above) per $100 \mu\text{m}^2$ of secondary and tertiary dendrites of WT and YAC128 CPNs: 8.8 ± 1.1 ($n = 37$; 2 cultures) and 6.8 ± 0.7 ($n = 57$; 3 cultures), respectively. Although synapse numbers were lower in YAC128 cultures, this did not reach statistical significance [$p = 0.1039$ (exact); Mann–Whitney test].

huntingtin protein expression affects AP-independent and -dependent glutamate release from CPN terminals.

To determine whether miniature glutamate release is enhanced at YAC128 CPN terminals targeting other CPNs, we measured CPN mEPSCs in WT and YAC128 cortical cultures with patch-clamp recordings at a series of DIV time points: 7, 14, 18, and 21. Both genotypes showed increased mEPSC frequencies as neurons

matured and formed synaptic connections with time in culture. However, YAC128 CPN mEPSC frequencies were consistently higher than age-matched WT controls after DIV7 and up until DIV21, at which point mEPSC frequencies became comparable between genotypes (Fig. 1A–L), as was also the case in the corticostriatal coculture model (Buren et al., 2016). The greatest genotype mEPSC difference occurred at DIV14, when mean YAC128 CPN

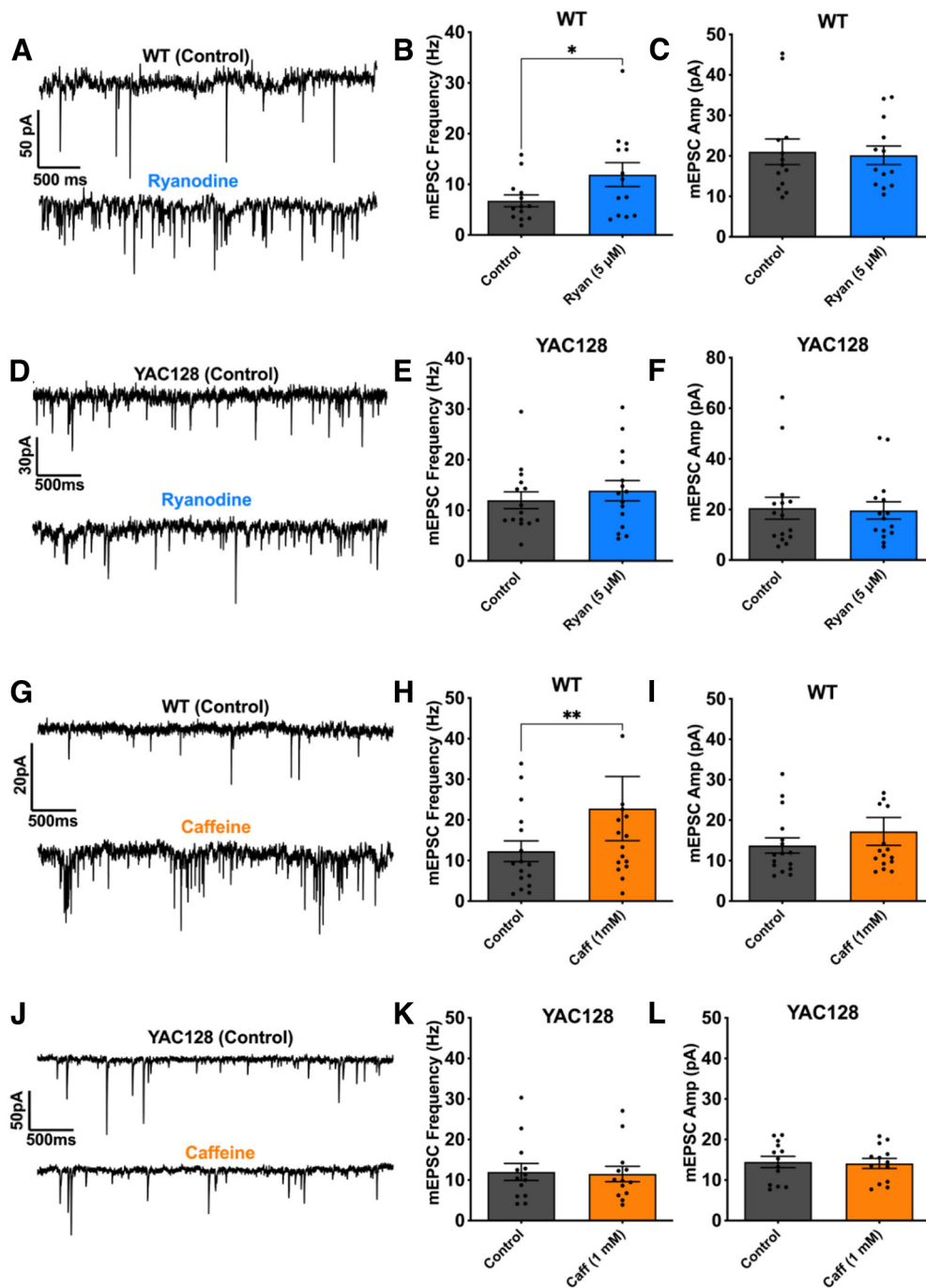


Figure 3. A Tonic ER Ca²⁺ leak elevates YAC128 pyramidal neuron mEPSC frequencies. **A, L**, Voltage-clamp recordings were made at -70 mV from DIV18 cultured WT (**A–C, G–I**) and YAC128 CPNs (**D–F, J–L**) in the presence of TTX (500 nM) and PTX (50 μM), under control conditions and during subsequent local ryanodine (5 μM) (**A–F**) or caffeine (1 mM) (**G–L**) application. In representative WT CPN traces, ryanodine (5 μM) (**A**), or caffeine (1 mM) (**G**), substantially increased the mEPSC frequency, whereas neither ryanodine (**D**) nor caffeine (**J**) appreciably altered mEPSC frequencies in representative YAC128 CPNs. Quantifying the population data revealed a significant ryanodine (5 μM)-mediated increase in mean mEPSC frequency in cultured WT CPNs (**B**) from 6.7 ± 1.2 Hz to 11.9 ± 2.4 Hz [$t_{(12)} = 2.50$; $p = 0.0280$; $n = 13$; 8 cultures; Student's paired t test], while caffeine (1 mM) significantly increased the mean mEPSC frequency in WT cultured CPNs (**K**) from 12.3 ± 2.5 Hz to 22.8 ± 8.0 Hz [$p = 0.0076$ (exact); $n = 16$; 8 cultures; Wilcoxon matched-pairs signed rank test]. Neither ryanodine (5 μM) nor caffeine (1 mM) significantly affected mean WT CPN mEPSC amplitudes: (**C**) (control: 21.0 ± 3.2 pA, ryanodine: 20.2 ± 2.3 pA) [$t_{(12)} = 0.65$; $p = 0.5278$; $n = 13$; 8 cultures; Student's paired t test], and (**I**) (control: 13.7 ± 1.9 pA, caffeine: 17.2 ± 3.4 pA) [$p = 0.8603$ (exact); $n = 16$; 8 cultures; Wilcoxon matched-pairs signed rank test] for ryanodine and caffeine experiments, respectively. YAC128 CPN frequencies were not significantly altered by either ryanodine (5 μM) (**E**) (control: 12.0 ± 1.7 Hz, ryanodine: 13.9 ± 2.0 Hz) [$t_{(14)} = 1.65$; $p = 0.1206$; $n = 15$; 4 cultures; Student's paired t test] or caffeine (1 mM) (**H**) (control: 12.0 ± 2.1 Hz, caffeine: 11.5 ± 1.9 Hz) [$t_{(12)} = 0.4808$; $p = 0.6393$; $n = 13$; 5 cultures; Student's paired t test]. Ryanodine (5 μM) and caffeine (1 mM) also did not significantly affect mean YAC128 CPN mEPSC amplitudes: (**F**) (control: 20.5 ± 4.4 pA, ryanodine: 19.6 ± 3.4 pA) [$t_{(14)} = 0.71$; $p = 0.4904$; $n = 15$; 4 cultures; Student's paired t test], and (**L**) (control: 14.5 ± 1.4 pA, caffeine: 14.1 ± 1.2 pA) [$t_{(12)} = 0.8086$; $p = 0.4345$; $n = 13$; 5 cultures; Student's paired t test] for ryanodine and caffeine experiments respectively. * $p < 0.05$. ** $p < 0.01$.

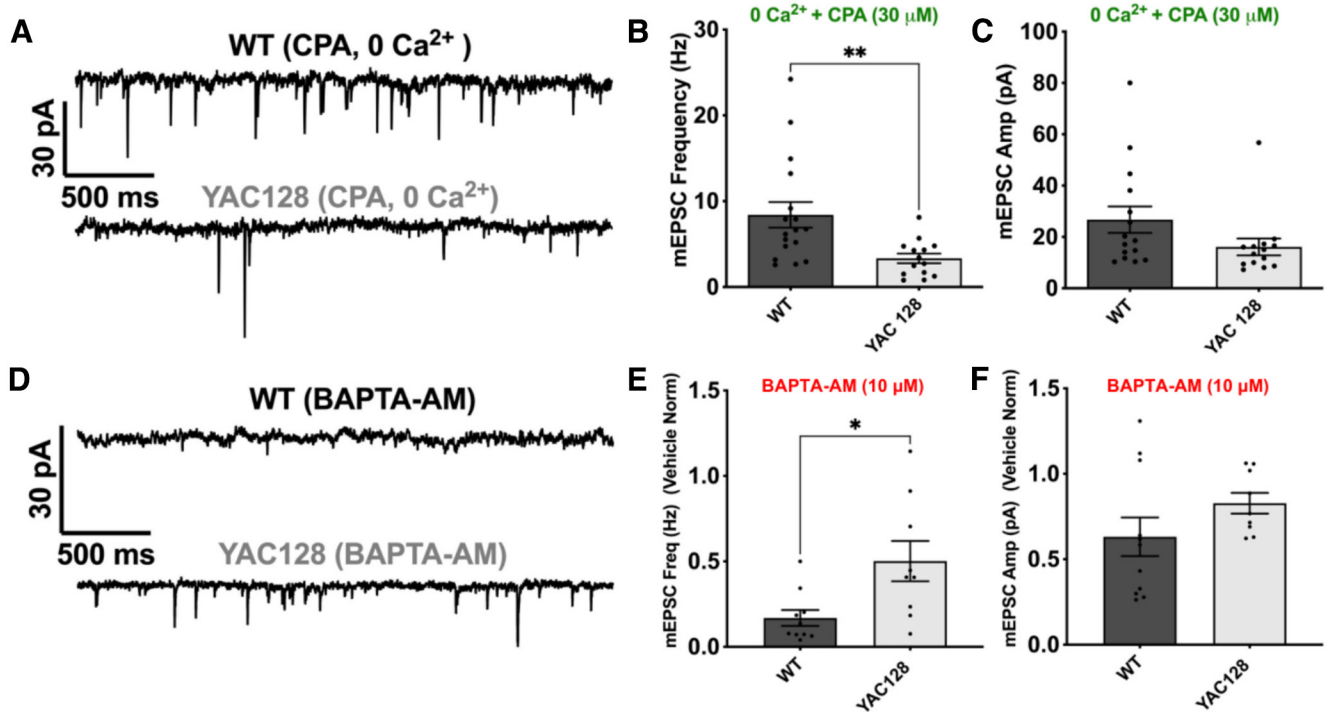


Figure 4. CPN mEPSCs in YAC128 cultures are more sensitive than WT to removal of extracellular Ca²⁺, but resistant to chelation of intracellular Ca²⁺ with BAPTA-AM. **A**, Voltage-clamp recordings from representative WT (top) and YAC128 (bottom) CPNs at -70 mV in the presence of TTX (500 nM) and PTX (50 μ M) (as before), with the addition of CPA (30 μ M) and in the absence of extracellular Ca²⁺. Note in all such recordings, CPNs were incubated in this CPA-containing, 0 mM Ca²⁺ ECSF for a minimum of 10 min. **B**, In CPA (30 μ M) and in the absence of extracellular Ca²⁺, YAC128 CPNs mEPSCs were significantly less frequent [3.3 ± 0.6 Hz ($n = 14$; 4 cultures)] compared with WT CPNs [8.4 ± 1.5 Hz ($n = 17$; 5 cultures)] under like conditions [$t_{(29)} = 2.952$; $p = 0.0062$; Student's unpaired t test]. **C**, In CPA (30 μ M) and in the absence of extracellular Ca²⁺, YAC128 CPNs showed a trend toward a lower mean mEPSC amplitude than in WT (WT: 26.7 ± 5.2 pA, YAC128: 16.1 ± 3.3 pA), but this did not reach statistical significance [$t_{(27)} = 1.706$; $p = 0.0995$; Student's unpaired t test]. **D**, Voltage-clamp recordings from representative WT (top) and YAC128 (bottom) CPNs preincubated in ECF containing BAPTA-AM (10 μ M) (for 30 min) at -70 mV in the presence of TTX (500 nM) and PTX (50 μ M) (as in **A**). Following BAPTA loading, cells were perfused in BAPTA-AM free ECF to washout extracellular BAPTA-AM. **E**, Preincubation in BAPTA-AM (10 μ M) reduced mean CPN mEPSC frequencies significantly more in WT than in YAC128 cultures. WT CPN showed $16.9 \pm 4.68\%$, whereas YAC128 showed $50.2 \pm 11.8\%$, the mean mEPSC frequencies observed in similar numbers of vehicle-treated paired CPN controls [WT treated with BAPTA ($n = 10$; 2 cultures); WT vehicle control ($n = 8$; 2 cultures); YAC128 treated with BAPTA ($n = 9$; 3 cultures); YAC128 vehicle control ($n = 10$; 3 cultures)] [$t_{(17)} = 2.731$; $p = 0.0176$; Student's unpaired t test]. **F**, Preincubation in BAPTA-AM did not differentially affect CPN mEPSC amplitudes in WT or YAC128 cultures [0.632 ± 0.113 vs 0.828 ± 0.061 for WT ($n = 10$; 2 cultures) and YAC128 ($n = 9$; 3 cultures), respectively (both normalized to the mean amplitudes of their genotype respective vehicle controls as in **E**)] [$t_{(18)} = 1.432$; $p = 0.0176$; Student's unpaired t test]. * $p < 0.05$. ** $p < 0.01$.

mEPSC frequencies were more than double that of WT: 10.83 ± 1.80 Hz versus 4.52 ± 0.60 Hz, respectively (Fig. 1D,E). YAC128 mEPSC frequencies remained significantly higher than WT at DIV18: 14.07 ± 1.54 Hz versus 9.92 ± 1.54 Hz, respectively (Fig. 1G, H). Age-matched YAC128 and WT CPNs showed similar mEPSC amplitudes across all DIV time points examined (Fig. 1C,F,I,L). We chose to perform subsequent experiments probing the mechanistic details underlying increased cortical mini glutamate release in DIV18 cortical monocultures, since this was the most mature culture stage at which mEPSC frequencies were elevated in YAC128 CPNs.

To test whether mHTT expression similarly affects mini glutamate release in a more physiologically representative preparation, we measured SPN mEPSCs in *ex vivo* cortical-striatal brain slices prepared from 2- to 4-month-old WT and YAC128 mice, time points when behaviorally evident disease is modest, if not absent (Slow et al., 2003). In these slices, YAC128 SPN mEPSC frequencies were approximately triple that of WT cells: 13.09 ± 3.06 Hz versus 4.33 ± 0.45 Hz respectively, while event amplitudes did not differ significantly between genotypes (Fig. 1M–O).

Synapse numbers and dendritic complexity are similar in WT and YAC128 cultured cortical pyramidal neurons at DIV18

The higher mEPSC frequencies seen in DIV18 YAC128 CPNs suggest an increased presynaptic glutamate release probability.

However, relative differences in synapse numbers could also account for this finding. To estimate numbers of synapses, we first expressed cytosolic GFP in a small proportion of neurons in WT and YAC128 cortical cultures and imaged full CPN dendritic arbors at DIV18. Sholl analysis revealed similar arborization patterns and total dendritic length in WT and YAC128 CPNs (Fig. 2A–D). In separate cultures, we expressed an internal GFP-tagged anti-PSD95 antibody (Gross et al., 2013) in a subset of neurons and immunostained for VGlut1 to identify glutamatergic synapses, and the GluA2 AMPAR subunit to identify functional synapses. Functional excitatory synapse numbers, defined here as GFP-labeled PSD95 puncta colocalized with VGlut1 and GluA2 immunofluorescent-labeled puncta, were not significantly different between DIV18 WT and YAC128 CPNs, although there was a trend toward lower synapse density in YAC128 CPNs (Fig. 2E,F). These results, together with the above data showing increased YAC128 CPN mEPSC frequencies at DIV18 (Fig. 1), point to increased miniature vesicular glutamate release from cortical terminals in YAC128 cultures.

Releasing ER calcium with low-dose ryanodine or caffeine increases the mEPSC frequency in WT, but not YAC128 cultures

Studies using mouse models suggest that Ca²⁺ release from ER stores is aberrant in HD because of increased IP₃ and ryanodine

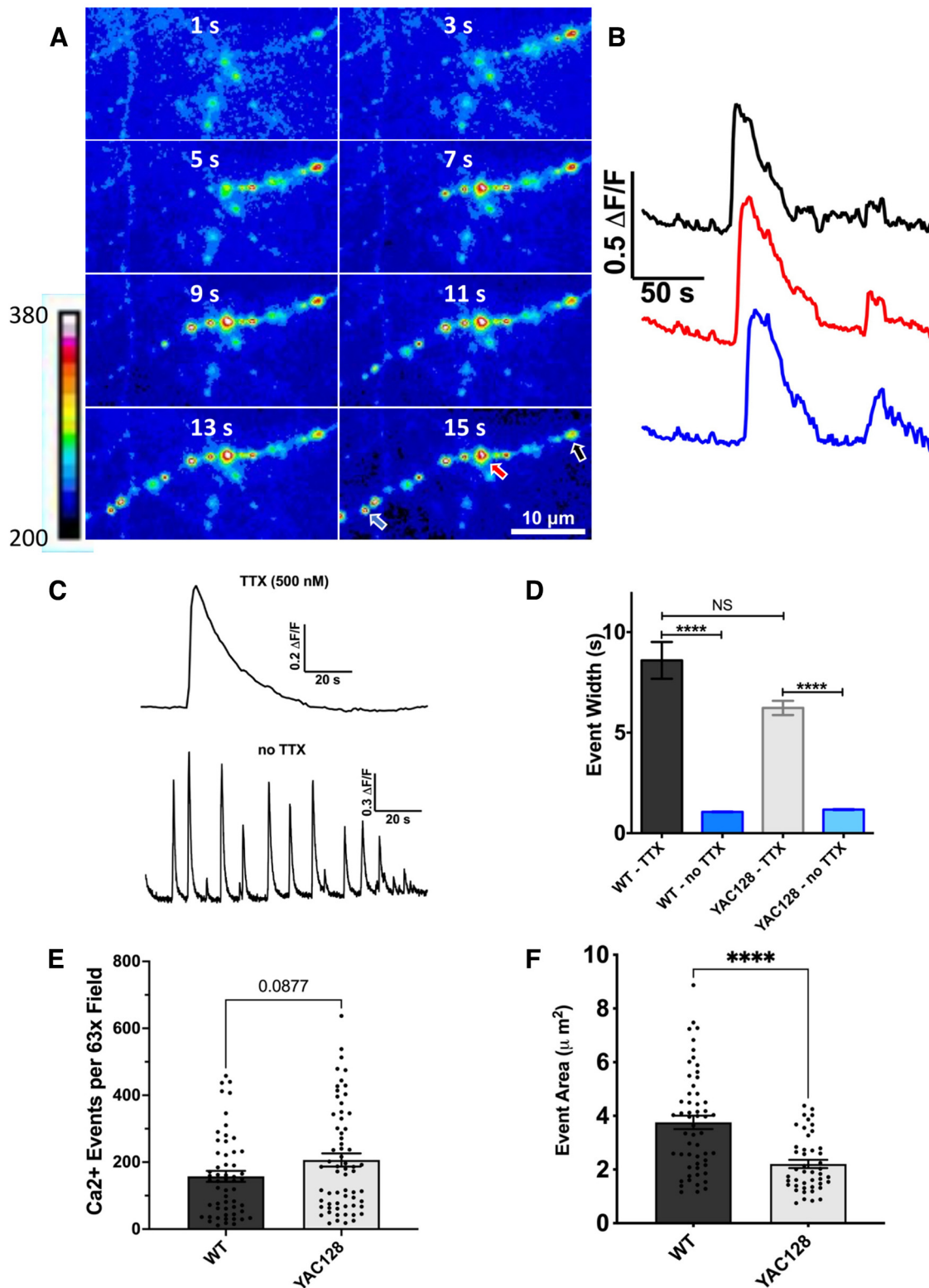


Figure 5. Slow miniature axonal Ca²⁺ waves are altered in YAC128 cortical cultures. **A**, Portion of a YAC128 rat synaptophysin-tagged GCaMP6-M (rSypH-GCaMP6m)-expressing axon during a miniature Ca²⁺ wave in the presence of ECF containing TTX (500 nM). Images represent raw GCaMP fluorescence values (arbitrary units) and comprise 15 s of a 4 min video. For illustrative purposes, images were binned temporally from the original 10 Hz movie, such that each 2 s frame reflects the average fluorescence of 20 successively acquired frames. **B**, Time course of ΔF/F (change in fluorescence over basal fluorescence) values extracted from 3 of the YAC128 rSypH-GCaMP6m-expressing axonal boutons (shown in **A** with color-coded arrows, panel labeled 15 s). Signals were spatially averaged across elliptical ROIs encompassing the indicated boutons and represent the entire 4 min imaging session. Note the multisecond delay in the propagation of signals between boutons and the prolonged time course of individual events. **C**, Representative 3 min ΔF/F time course from a WT rSypH-GCaMP6m-expressing axonal bouton in TTX (500 nM) (top). Note the substantially longer duration of this miniature event compared with representative spontaneous events recorded without TTX from a separate WT rSypH-GCaMP6m-expressing bouton (bottom). **D**, Average half amplitude width of spontaneous Ca²⁺ events occurring in rSypH-GCaMP6m-expressing boutons in WT and YAC128 cortical cultures in the presence and absence of TTX (500 nM). Select comparisons were made with the Mann–Whitney test because event widths in all groups failed the D’Agostino–Pearson omnibus normality test. WT events were

receptor activity (Tang et al., 2003; Suzuki et al., 2012). Although effects of mHTT on the presynaptic ER have not been specifically studied, we hypothesized that a presynaptic ER Ca²⁺ leak contributes to the elevated miniature glutamate release seen in our YAC128 cultures. To test this hypothesis, we first recorded mEPSCs before and during local application of low-dose (5 μ M) ryanodine to cultured CPNs; 5 μ M ryanodine releases ER Ca²⁺ by opening ryanodine receptors (Meissner, 2017). In WT cultures, 5 μ M ryanodine nearly doubled the CPN mEPSC frequency: from 6.74 ± 1.17 Hz to 11.91 ± 2.36 Hz [Students' paired *t* test; $p = 0.0280$; $n = 13$ cells] (Fig. 3A–C). However, in YAC128 cultures, ryanodine (5 μ M) did not significantly alter the CPN mEPSC frequency: 11.98 ± 1.66 Hz versus 13.89 ± 2.01 Hz, under control conditions and in ryanodine (5 μ M), respectively (Fig. 3D–F), suggesting that the effect of ryanodine was occluded in YAC128 cultures. A comparison of the percent change in mEPSC frequency following ryanodine (5 μ M) revealed a significantly greater response in WT than in YAC128 CPNs [$31.7 \pm 7.5\%$ ($n = 13$) versus $5.2 \pm 9.5\%$ ($n = 15$) in WT and YAC128 CPNs, respectively (Students' unpaired *t* test; $p = 0.0418$)]. We next used caffeine (1 mM) as an alternative means of agonizing ryanodine receptors; this more prominently increased the mEPSC frequency in WT cultures but otherwise produced similar results [WT: $99.2 \pm 34.1\%$ increase in mEPSC frequency ($n = 16$; 8 cultures), versus YAC128: $1.2 \pm 7.6\%$ increase in mEPSC frequency ($n = 13$; 5 cultures)] [$p = 0.0025$ (exact); Mann–Whitney test] (Fig. 3G–L). Neither ryanodine nor caffeine altered mEPSC amplitude in either genotype (Fig. 3C,F,I,L).

YAC128 mEPSCs are more sensitive to removal of extracellular Ca²⁺ but resistant to chelation of intracellular Ca²⁺

We next reasoned that, if an ongoing release of presynaptic ER Ca²⁺ in YAC128 cultures occludes potentiation of miniature glutamate release by low-dose ryanodine and caffeine, inhibiting ER Ca²⁺ release should lower YAC128 miniature event frequencies to WT levels. To test this, we pre-incubated cultures with ECF containing the sarco/endoplasmic reticulum Ca²⁺-ATPase (SERCA) pump inhibitor cyclopiazonic acid (CPA) (30 μ M) to deplete ER Ca²⁺ stores. Since ER Ca²⁺ depletion can increase cytosolic Ca²⁺ by engaging the SOC response, and this effect can increase mini neurotransmitter release (Emptage et al., 2001; Chanaday et al., 2021), we performed these experiments in the absence of extracellular Ca²⁺. Surprisingly, under these conditions, mean mEPSC frequencies were significantly lower in YAC128 CPNs compared with WT [3.33 ± 0.57 Hz ($n = 14$) vs

8.41 ± 1.50 Hz ($n = 17$), respectively (Student's unpaired *t* test; $p = 0.0062$] (Fig. 4A–C), suggesting that YAC128 mini glutamate release is far more dependent on extracellular Ca²⁺ and/or release from ER stores. If the above conditions fully deprived neurons of presynaptic Ca²⁺, this result might indicate a lower intrinsic (Ca²⁺-independent) synaptic vesicle release probability in YAC128, versus WT, cultures. However, remaining synaptic events can still be Ca²⁺-dependent, as pharmacological SERCA pump inhibition has been reported to only partially deplete the axonal ER Ca²⁺ (de Juan-Sanz et al., 2017). Alternatively, mini release in YAC128 cultures could be more dependent on extracellular Ca²⁺ because of a greater role of CaSR signaling (Vyleta and Smith, 2011) or SOC-mediated Ca²⁺ entry (Chanaday et al., 2021). To address these possibilities, we loaded WT and YAC128 cortical cultures with the cell membrane-permeant Ca²⁺ chelator BAPTA-AM and measured CPN mEPSCs in standard ECF (after extracellular BAPTA-AM washout). WT CPN mEPSC frequencies were significantly more sensitive to reduced intracellular Ca²⁺ than YAC128 CPNs ($16.9 \pm 4.6\%$ that of vehicle controls in WT ($n = 10$) vs $50.2 \pm 11.8\%$ in YAC128 ($n = 9$); Students' unpaired *t* test; $p = 0.0142$) (Fig. 4D,E). Their near complete block by BAPTA-AM indicates that WT mEPSCs are highly dependent on intracellular Ca²⁺, whereas YAC128 mEPSCs are far less so. Presumably, this reduced intracellular Ca²⁺ dependency also means that the substantial reduction of YAC128 mEPSC frequencies in CPA and 0 Ca²⁺ was due primarily to the absence of extracellular Ca²⁺ rather than pharmacological SERCA pump inhibition.

Presynaptic Ca²⁺ sparks and waves are altered in YAC128 cultures

To directly monitor presynaptic Ca²⁺ dynamics, we next exploited a genetically encoded Ca²⁺ sensor that preferentially localizes to presynaptic terminals, created by fusing GCaMP6-M with the rat synaptophysin protein via a small glycine-serine linker (rSypH-GCaMP6m) (Chen et al., 2013). We expressed rSypH-GCaMP6m in cultured cortical neurons and performed Ca²⁺ imaging experiments, first in the presence of TTX (500 nM) to relate presynaptic Ca²⁺ signaling to our mEPSC findings (above). For clarity, we will refer to axonal Ca²⁺ events in TTX (AP-independent) as miniature, and events present in the absence of TTX (both activity-dependent and -independent) as spontaneous. Both YAC128 and WT cultures showed miniature axonal Ca²⁺ events, as well as slow Ca²⁺ waves traversing multiple neighboring boutons (Fig. 5A,B). In some cases, these axonal waves traveled extensively, crossing entire $63 \times (178.6 \mu\text{m} \times 113.1 \mu\text{m})$ imaging fields over multiple seconds; in contrast, spontaneous Ca²⁺ events seen in the absence of TTX (i.e., AP-dependent) could not be temporally resolved owing to relatively slow GCaMP kinetics and appeared simultaneously across all imaged boutons of a given axon. Miniature presynaptic Ca²⁺ events imaged in TTX were also strikingly long lasting, on average 5–10 times longer than typical events seen in the absence of TTX (Fig. 5C,D). We first quantified these AP-independent miniature axonal Ca²⁺ events with the AQUA, an ROI-agnostic algorithm that detects waves as suprathreshold signals connected in time and space (Wang et al., 2019). Such waves varied considerably between culture batches; and although more were detected on average in YAC128 cultures, this effect did not reach statistical significance (Fig. 5E). Interestingly, Ca²⁺ waves tended to travel further in WT than YAC128 axons, reflected in a significantly larger mean event area (Fig. 5F).

In subsets of WT and YAC128 cultures, we identified boutons from presumptive glutamatergic synapses, by coexpressing an

←

significantly longer with TTX [8.60 ± 0.92 s ($n = 164$ events; 85 boutons; 4 cultures)] than without [1.06 ± 0.97 s ($n = 3725$ events; 175 boutons; 4 cultures)] [$p < 0.0001$ (approximate); Mann–Whitney test]. Likewise, YAC128 half widths were significantly longer with TTX [6.23 ± 0.35 s ($n = 440$ events; 153 boutons; 4 cultures)] than without [1.17 ± 1.46 s ($n = 5159$ events; 422 boutons; 6 cultures)] [$p < 0.0001$ (approximate); Mann–Whitney test]. **E**, Numbers of miniature axonal events (as in **A,B**) during 3 min recordings of $63 \times$ objective ($178.6 \mu\text{m} \times 113.1 \mu\text{m}$) detected with the AQUA software. Miniature axonal Ca²⁺ events were detected more frequently in YAC128 cortical cultures [206.4 ± 19.6 events/3 min ($n = 56$ fields; 11 cultures)], compared with WT [157.5 ± 16.3 events/3 min ($n = 63$ fields; 12 cultures)]; however, this difference did not reach statistical significance [$p = 0.0877$ (exact); Mann–Whitney test]. **F**, The average area of miniature axonal Ca²⁺ events imaged in a given $63 \times$ objective field over 3 min from WT and YAC128 cortical cultures detected as in **E** was significantly reduced in YAC128 cultures [$2.206 \pm 0.154 \mu\text{m}^2$ ($n = 45$ fields; 7 cultures)] compared with WT [$3.757 \pm 0.250 \mu\text{m}^2$ ($n = 56$ fields; 8 cultures)] [$p = 0.0001$ (exact); Mann–Whitney test]. **** $p < 0.0001$.

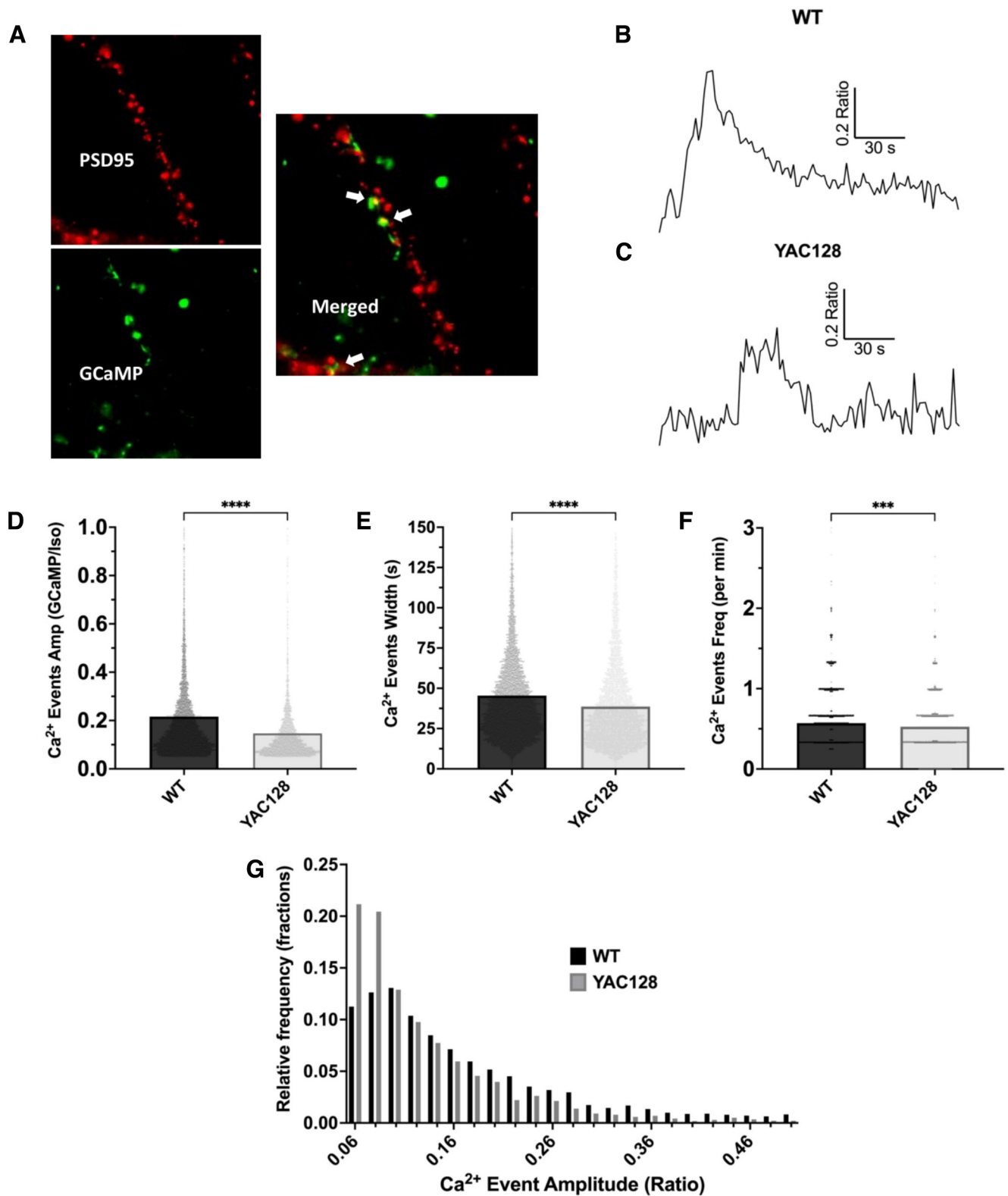


Figure 6. Miniature Ca²⁺ events at boutons of glutamatergic synapses are substantially smaller in YAC128 cortical cultures. **A**, Representative portion of a 63× fluorescence microscopy image (37.2 μm × 37.2 μm shown) from a WT cortical culture, in which neurons expressed both a genetically encoded mCherry-tagged-PSD95 (to label CPN dendritic spines) (red channel, top left) and rSyph-GCaMP6m (to measure Ca²⁺ activity at axonal boutons) (green channel, bottom left). A CPN dendritic segment is in view with mCherry-PSD95-labeled spines visible as red puncta, along with one or more rSyph-GCaMP6m-expressing axons with boutons visible as green puncta. The merged red-green channel (middle right) reveals yellow puncta (highlighted with arrows) representing colocalizations between rSyph-GCaMP6m-expressing boutons and mCherry-PSD95-tagged spines; our custom MATLAB software identified such colocalizations (methods) and restricted analysis of rSyph-GCaMP6m signals to these boutons. **B**, **C**, Fluorescence time courses from representative WT (**B**) and YAC128 (**C**) rSyph-GCaMP6m-expressing boutons (both colocalized with mCherry-PSD95-tagged dendritic spines), showing clear miniature Ca²⁺ events in TTX (500 nM). Time courses were generated by dividing standard GCaMP fluorescence (excited with 488 nm light) by isobestic point fluorescence (excited with 405 nm light), so that the resultant signal is normalized for GCaMP expression. **D**, Amplitudes of miniature Ca²⁺ events at mCherry-PSD95 colocalized boutons (as in **B**) were significantly lower in YAC128 cortical cultures [0.1465 ± 0.0025 488F/405F (*n* = 3836 boutons; 6 cultures)] compared with WT [0.2160 ±

mCherry-tagged PSD95 construct and restricting GCaMP analysis to rSyph-GCaMP6m-labeled boutons clearly colocalized with mCherry-labeled puncta (Fig. 6A). As in the larger rSyph-GCaMP6m-labeled bouton population (including those of GABA interneurons), numerous PSD95 colocalized boutons were active in the presence of TTX in cultures of both genotypes (Fig. 6B,C). To systematically compare miniature event amplitudes between genotypes in these experiments, we capitalized on the ability to measure GCaMP fluorescence independent of its Ca²⁺-bound state by exciting it with light at its isosbestic frequency (~405 nm) (Barnett et al., 2017). By normalizing GCaMP traces to isosbestic fluorescence intensity, we thereby accounted for any differences in GCaMP expression between cultures and individual boutons. These experiments revealed the amplitudes of miniature Ca²⁺ events were, on average, 32% smaller in YAC128 boutons (Fig. 6D). YAC128 miniature events were also significantly shorter in duration when measured at half amplitude (Fig. 6E). In contrast to analysis using the AQuA algorithm (above), miniature event frequencies were slightly, but significantly, lower in mCherry-colocalized YAC128 boutons (Fig. 6F). However, inspection of the Ca²⁺ event amplitude distributions from both genotypes revealed highly skewed distributions with modes (or distribution peaks) very near the event-amplitude detection threshold (Fig. 6G). These results suggest a significant number of smaller amplitude events may not have been detected amid trace noise and that YAC128 cultures would be more susceptible to undercounting of such events, given the smaller average YAC128 event amplitude.

Responses to the Ca²⁺ ionophore ionomycin are reduced in YAC128 presynaptic boutons

The brightness of GCaMP fluorescence at a given excitation light intensity is determined both by its expression level and the degree of its Ca²⁺ binding. Quantitative Ca²⁺ concentration comparisons are therefore best made when an additional calibration step is performed to account for differential GCaMP expression at individual ROIs. To do so, in subsets of experiments we permeabilized neuronal membranes to Ca²⁺ with the Ca²⁺ ionophore ionomycin following GCaMP imaging. This theoretically allowed GCaMP fluorescence to be measured in the presence of the known extracellular Ca²⁺ concentration (2 mM for these experiments) and for differences in GCaMP expression to be inferred based on the differential fluorescence intensity of ROIs under these conditions.

Boutons in YAC128 cultures responded to ionomycin (10 μM) application with significantly smaller fluorescence intensity increases (ΔF/F) compared with WT (Fig. 7A–C), a finding that would be consistent with higher resting cytosolic Ca²⁺ in YAC128 boutons (Lindhout et al., 2019). Furthermore, in both genotypes, ionomycin-mediated changes in presynaptic GCaMP fluorescence were significantly smaller in boutons showing at least one miniature Ca²⁺ event in the previous 3 min recording (Fig. 7D–F),

←

0.0031 488F/405F ($n = 7478$ boutons; 7 cultures) [$p < 0.0001$ (approximate); Mann–Whitney test]. **E**, Miniature Ca²⁺ event widths (or durations) at mCherry-PSD95 colocalized boutons (as in **B**), calculated at half the peak event amplitude, were significantly shorter in YAC128 cortical cultures [38.63 ± 0.41 s ($n = 4257$ boutons; 6 cultures)] compared with WT [45.45 ± 0.35 s ($n = 8376$ boutons; 7 cultures)] [$p < 0.0001$ (approximate); Mann–Whitney test]. **F**, Miniature Ca²⁺ events at mCherry-PSD95 colocalized boutons (as in **B**), were significantly less frequent in YAC128 cortical cultures [0.5261 ± 0.0058 events/min ($n = 4380$ boutons; 6 cultures)] compared with WT [0.5709 ± 0.0043 events/min ($n = 8411$ boutons; 7 cultures)] [$p = 0.0002$ (approximate); Mann–Whitney test]. **G**, Distributions of WT (black) and YAC128 (gray) miniature Ca²⁺ event amplitudes (from **D**) using a bin width of 0.02 488F/405F. *** $p < 0.001$. **** $p < 0.0001$.

suggesting that higher basal cytosolic Ca²⁺ concentrations occur in a population of boutons undergoing TTX-resistant Ca²⁺ events. Interpretations were confounded, however, by the observation that cytosolic Ca²⁺ responses typically peaked following ionomycin application then rapidly declined (Fig. 7A,B), inconsistent with the plateau expected if cytosolic bouton Ca²⁺ levels truly equilibrated with the 2 mM extracellular Ca²⁺ concentration. Several studies suggest a more complex mechanism of ionomycin's actions on cytosolic Ca²⁺ concentrations, with a critical involvement of ER Ca²⁺ release and subsequent SOC entry (Morgan and Jacob, 1994; Müller et al., 2013). Moreover, some evidence suggests that ionomycin's mechanism of action varies considerably with its concentration. We therefore repeated the above experiments with a higher (60 μM) ionomycin dose, and in subsets of these experiments, recorded for a longer duration following ionomycin treatment (6–8 vs 2 min) to see if Ca²⁺ responses eventually plateaued. Despite a 6 × increase in dose, we observed similar results to those seen with the 10 μM ionomycin (Fig. 7G,H).

GCaMP isosbestic point measurements suggest that resting cytosolic Ca²⁺ levels are not elevated in YAC128 presynaptic boutons

We next used isosbestic measurements as an alternative means to calibrate GCaMP expression at individual boutons (as above) and to test whether reduced GCaMP Ca²⁺ responses to 10 and 60 μM ionomycin were best explained by depleted bouton ER Ca²⁺ stores or indeed reflect higher resting cytosolic Ca²⁺ concentrations in YAC128 boutons. We first verified that GCaMP isosbestic point fluorescence intensity measurements were independent of the cytosolic Ca²⁺ concentrations under our imaging conditions. In recordings where we rapidly switched between isosbestic (405 nm excitation) and conventional GCaMP (480 nm excitation) measurements, isosbestic time courses showed similar bleaching dynamics to that of the corresponding GCaMP trace, but were of a lower fluorescence intensity and importantly lacked the Ca²⁺ transients seen in the GCaMP traces (Fig. 7I). Transient artifacts were commonly seen in the isosbestic channel following ionomycin (60 μM) application. These manifested as either small increases in signal (as in Fig. 7I) that occurred throughout the entire imaging field, or a small reduction in signal because of bouton swelling or movement causing some GCaMP signal to move out of the analysis ROI. In either case, normalizing GCaMP traces to the isosbestic channel helped to compensate for these artifacts; and subsequently, ionomycin responses typically did plateau (Fig. 7J,K). However, this ionomycin response plateau was still typically preceded by a substantially larger rise in Ca²⁺. Furthermore, if ionomycin application freely permeabilized the cell membrane to Ca²⁺ (thus equilibrating intracellular and extracellular compartments), GCaMP/isosbestic measurements in ionomycin should depend only the extracellular Ca²⁺ concentration and not differ between genotypes. However, GCaMP/isosbestic values following ionomycin (60 μM) remained significantly larger in WT than YAC128 boutons (Fig. 7L).

Surprisingly, resting GCaMP/isosbestic measurements were significantly lower in YAC128 boutons (Fig. 7J,K,M), a result suggesting lower basal cytosolic Ca²⁺, as opposed to the higher resting cytosolic Ca²⁺ concentrations expected. Together, these results suggest that reduced ionomycin responses in YAC128 boutons are because of decreased ER Ca²⁺ content and not differences in the cytosolic Ca²⁺ concentration. Reduced ionomycin responses in boutons showing miniature Ca²⁺ events in both genotypes may therefore reflect ER Ca²⁺ depletion because of ongoing ER release.

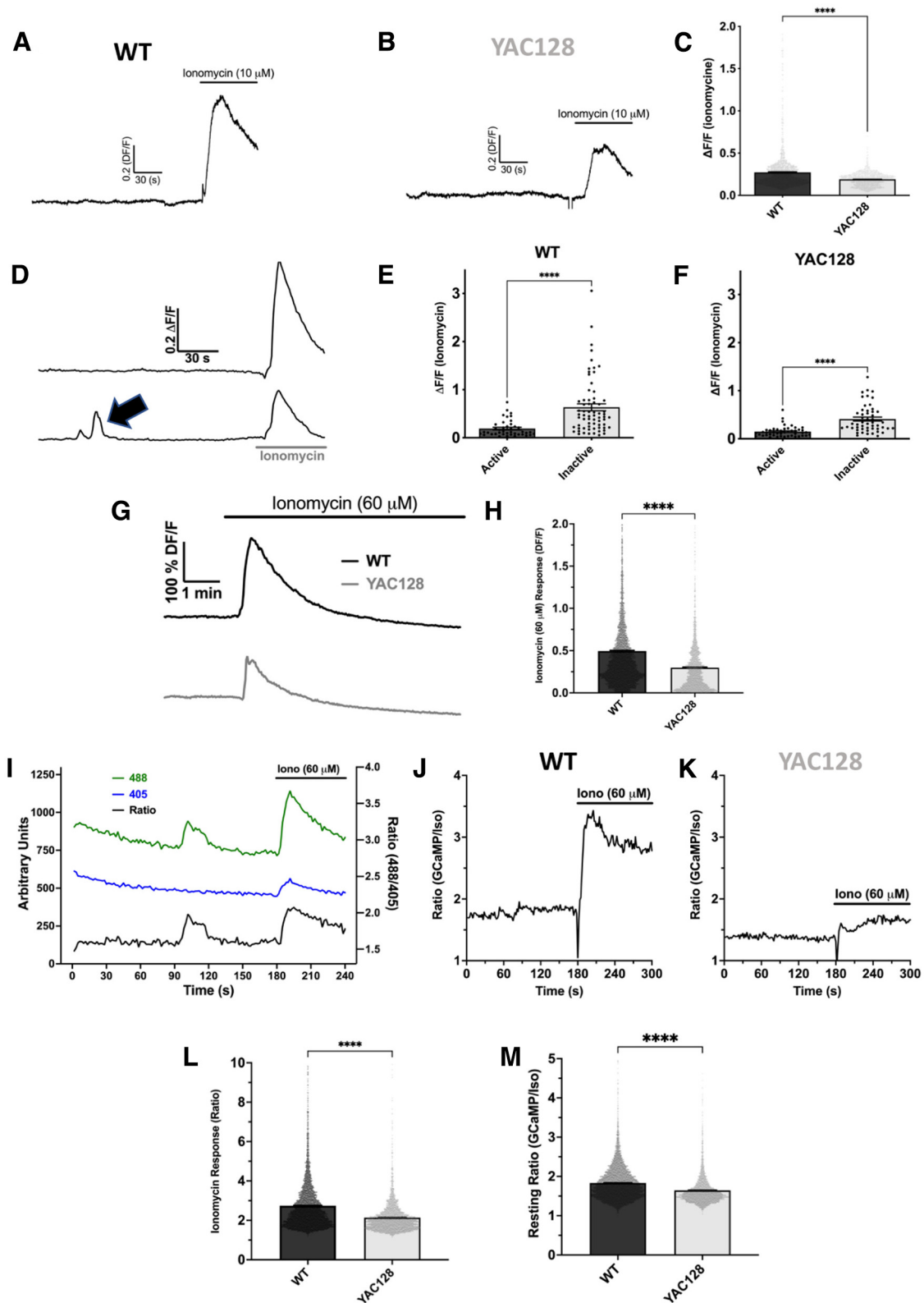


Figure 7. Ionomycin responses and isosbestic point GCaMP calibrations suggest that axonal ER Ca²⁺ is depleted in YAC128 cortical cultures. **A, B**, Four minute DF/F traces from rSyph-GCaMP6m-expressing axonal boutons in representative WT (**A**) and YAC128 (**B**) cortical cultures imaged under standard conditions (in TTX 500 nM), before and following treatment with ionomycin (10 μM) (at the 3 min mark). **C**, Ionomycin responses of all WT and YAC128 rSyph-GCaMP6m-expressing axons automatically detected with the AQUA software suite (for reference, see Materials and Methods). The WT bouton population showed a significantly greater ionomycin-mediated change in fluorescence [0.272 ± 0.006 DF/F ($n = 1681$ boutons; 4 cultures)] compared with the YAC128 population [0.190 ± 0.002 DF/F ($n = 1462$ boutons; 4 cultures)] [$p < 0.0001$ (exact); Mann–Whitney test]. **D**, DF/F time courses from two rSyph-GCaMP6m-expressing axonal boutons from a representative YAC128 culture in the presence of TTX (500 nM). The first bouton (top) is inactive during the 3 min imaging session, while the second bouton (bottom) shows a clear miniature Ca²⁺ event (black arrow). Subsequent application of the Ca²⁺ ionophore ionomycin (10 μM) elicits a smaller Ca²⁺ response in the active bouton. **E, F**, Ionomycin responses of rSyph-GCaMP6m-expressing boutons in the presence of TTX following a 3 min imaging session in WT (**E**) and YAC128 (**F**) cultures. Boutons were classified as active or inactive based on the

Caffeine increases basal Ca²⁺ and miniature events in WT, but not YAC128 cortical boutons

The slow kinetics of the above miniature presynaptic Ca²⁺ events are consistent with ER-mediated Ca²⁺ waves reported in postsynaptic neuronal compartments (Ross, 2012). We next tested whether these presynaptic Ca²⁺ events were affected by caffeine (1 mM), an ER ryanodine receptor agonist that substantially increased mEPSC frequencies in WT, but not YAC128 cultures (above). In the presence of TTX, caffeine (1 mM) significantly increased the presynaptic Ca²⁺ event frequency in WT cultures (Fig. 8A) but did not significantly alter event frequencies in YAC128 cultures (Fig. 8B).

When exploring the effects of caffeine (and other pharmacological agents; see below) on miniature axonal Ca²⁺ events, we compared separate imaging fields to minimize impacts of photobleaching and toxicity. However, we observed relatively rapid changes in basal rSypH-GCaMP6m fluorescence in response to caffeine (1 mM) application, conducive to within-bouton measurements. A clear increase in basal rSypH-GCaMP6m fluorescence was seen in most WT boutons following caffeine (1 mM) application, which was attenuated in YAC128 boutons (Fig. 8C). This caffeine (1 mM)-mediated increase in rSypH-GCaMP6m fluorescence was significantly greater in WT than in YAC128 boutons (Fig. 8D), consistent with depleted ER Ca²⁺ stores in YAC128 CPNs, as suggested by the results of the ionomycin experiments.

CPA increases miniature axonal Ca²⁺ event frequencies and reduces ionomycin responses in WT, but not YAC128 cortical boutons

Pharmacological inhibition of the ER SERCA pump has been shown to increase presynaptic cytosolic Ca²⁺ concentrations and

←

presence, or lack thereof, of at least one miniature Ca²⁺ event during the initial 3 min recording. Ionomycin responses were significantly larger in the population of inactive boutons [WT: 0.633 ± 0.072 DF/F (*n* = 67 boutons); YAC128: 0.410 ± 0.040 DF/F (*n* = 51 boutons)], versus active boutons [WT: 0.191 ± 0.026 DF/F (*n* = 41 boutons), *p* < 0.0001 (exact) by Mann–Whitney test; YAC128: 0.149 ± 0.016 DF/F (*n* = 46 boutons), *p* < 0.0001 (exact) by Mann–Whitney test]. Four cultures for WT and four cultures for YAC128. **G**, Eight minute DF/F traces from rSypH-GCaMP6m-expressing axonal boutons in representative WT (top black) and YAC128 (bottom gray) cortical cultures imaged under standard conditions (in TTX 500 nM), before and following treatment with ionomycin (60 μM) (at the 2 min mark). **H**, Peak DF/F Ca²⁺ responses to ionomycin (60 μM) were significantly larger in WT boutons [0.4955 ± 0.0084 DF/F (*n* = 5740 boutons; 6 cultures)] compared with YAC128 [0.2980 ± 0.0065 DF/F (*n* = 3663 boutons; 5 cultures)] [*p* < 0.0001 (approximate); Mann–Whitney test]. Analysis was restricted to GCaMP6m-expressing boutons colocalized with mCherry-PSD95-tagged dendritic spines here and for **L, M, J**. **J**, Fluorescence intensity traces from a representative WT rSypH-GCaMP6m-expressing bouton in which we rapidly switched between Ca²⁺-dependent measurements with 488 nm excitation (green trace) and isosbestic (or Ca²⁺-independent) measurements with 405 nm excitation (blue trace). For analysis, the Ca²⁺-dependent (488 nm) trace was divided by the isosbestic (405 nm) trace (black trace), thereby accounting for differences in GCaMP expression and illumination levels between experiments. **J, K**, Five minute ratio (488 nm/405 nm) traces (as in **J**) from representative WT (**J**) and YAC128 (**K**) GCaMP6m-expressing boutons (colocalized with mCherry-PSD95-tagged dendritic spines) in the presence of TTX (500 nM). Ionomycin (60 μM) was applied to both boutons at the 3 min mark. The larger ionomycin response amplitude in the WT bouton along with the higher resting fluorescence in the WT bouton before the ionomycin application, suggesting higher resting Ca²⁺ levels. **L**, Peak ratio (488F/405F) Ca²⁺ responses to ionomycin (60 μM) were significantly larger in WT boutons [2.734 ± 0.018 488F/405F (*n* = 5740 boutons; 6 cultures)] compared with YAC128 [2.132 ± 0.013 488F/405F (*n* = 3663 boutons; 5 cultures)] [*p* = 0.0001 (approximate); Mann–Whitney test]. **M**, Resting ratio (488F/405F) fluorescence levels (calculated as the minimum value in each bouton trace, see Materials and Methods) was significantly higher in WT boutons [1.832 ± 0.0050 488F/405F (*n* = 8410 boutons; 7 cultures)] compared with YAC128 [1.643 ± 0.0060 488F/405F (*n* = 4379 boutons; 6 cultures)] [*p* = 0.0016 (exact); Mann–Whitney test]. *****p* < 0.0001.

potentiate miniature glutamate release. We next tested whether SERCA pump inhibition with CPA differentially impacts axonal Ca²⁺ in WT versus YAC128 cultures. WT cultures incubated with CPA (30 μM) in the presence of TTX (500 nM) showed significantly more miniature axonal Ca²⁺ events (vs experiments in TTX alone) (Fig. 8E), whereas axonal Ca²⁺ event frequencies did not significantly differ between YAC128 cultures in CPA and TTX (vs TTX alone) (Fig. 8F). In WT cultures pre-incubated with CPA (30 μM) and TTX, responses to ionomycin (60 μM) were significantly reduced by 43% (vs responses in TTX alone) (Fig. 8G). Conversely, pre-incubation with CPA did not significantly alter ionomycin responses in YAC128 boutons (Fig. 8H), which showed similar amplitude responses to WT after CPA treatment. These results further support that ER Ca²⁺ is depleted in YAC128 cortical axons. As expected, CPA also increased cytosolic Ca²⁺ in WT boutons, as reflected by increased resting GCaMP/isosbestic values (data not shown). However, this effect was more complex in 2 of 3 cultures tested, in which the GCaMP/isosbestic decreased substantially below the baseline value following prolonged (>60 min) CPA incubation.

Activity-dependent Ca²⁺ transients in presynaptic cortical terminals are less frequent in YAC128 cultures because of reduced AP firing rates

We next used the rSypH-GCaMP6m construct in the absence of TTX to examine presynaptic AP-dependent Ca²⁺ transients in WT and YAC128 cortical cultures. When neuronal AP firing was intact, rSypH-GCaMP6m-expressing boutons in both WT and YAC128 cultures were dominated by presumably VGCC-mediated signals (Fig. 9A,B). These spontaneous signals were more frequent than those seen in the presence of TTX, but of far shorter duration. Interestingly, these spontaneous Ca²⁺ events were nearly twice as frequent in WT axonal boutons, compared with those in YAC128 cultures (Fig. 9A,B,E). Ryanodine (5 μM) modestly but significantly reduced the frequency of these events in WT cultures (by 17%) (Fig. 9A,C,E). Conversely, 5 μM ryanodine elicited a small, but significant increase in the frequency of these events in YAC128 cultures (Fig. 9B,D,E). Although it has been reported that axonal ER Ca²⁺ can be released following AP-mediated presynaptic Ca²⁺ influx (Emptage et al., 2001), amplitudes of AP-dependent Ca²⁺ events were not significantly lower in YAC128 boutons, as might be expected if ER Ca²⁺ was a major contributor to these signals in WT, but not YAC128, boutons. Alternatively, reduced AP-dependent axonal Ca²⁺ event frequencies could be explained by lower YAC128 CPN AP firing rates. To test this possibility, we expressed cytosolic GCaMP 7f in cultured cortical neurons and recorded AP-dependent Ca²⁺ events from the soma of transfected CPNs. Frequencies of such activity-dependent somatic signals were significantly lower in YAC128 versus WT CPNs (Fig. 9F,G), suggesting that lower activity-dependent axonal Ca²⁺ event frequencies in YAC128 cultures are mediated by decreased CPN AP firing rates rather than a specifically axon-localized mechanism. Activation of a Ca²⁺-dependent K⁺ conductance following release of ER Ca²⁺ stores is a plausible, although highly speculative, explanation for reduced YAC128 CPN AP firing and ryanodine's effects on WT spontaneous axonal Ca²⁺ events. The small but significant reduction in spontaneous Ca²⁺ events in YAC128 boutons following ryanodine treatment is more puzzling, but perhaps explained by ryanodine-mediated RyR closure predominating in YAC128 CPN, a plausible scenario if the YAC128 RyR population normally favors the open conformation.

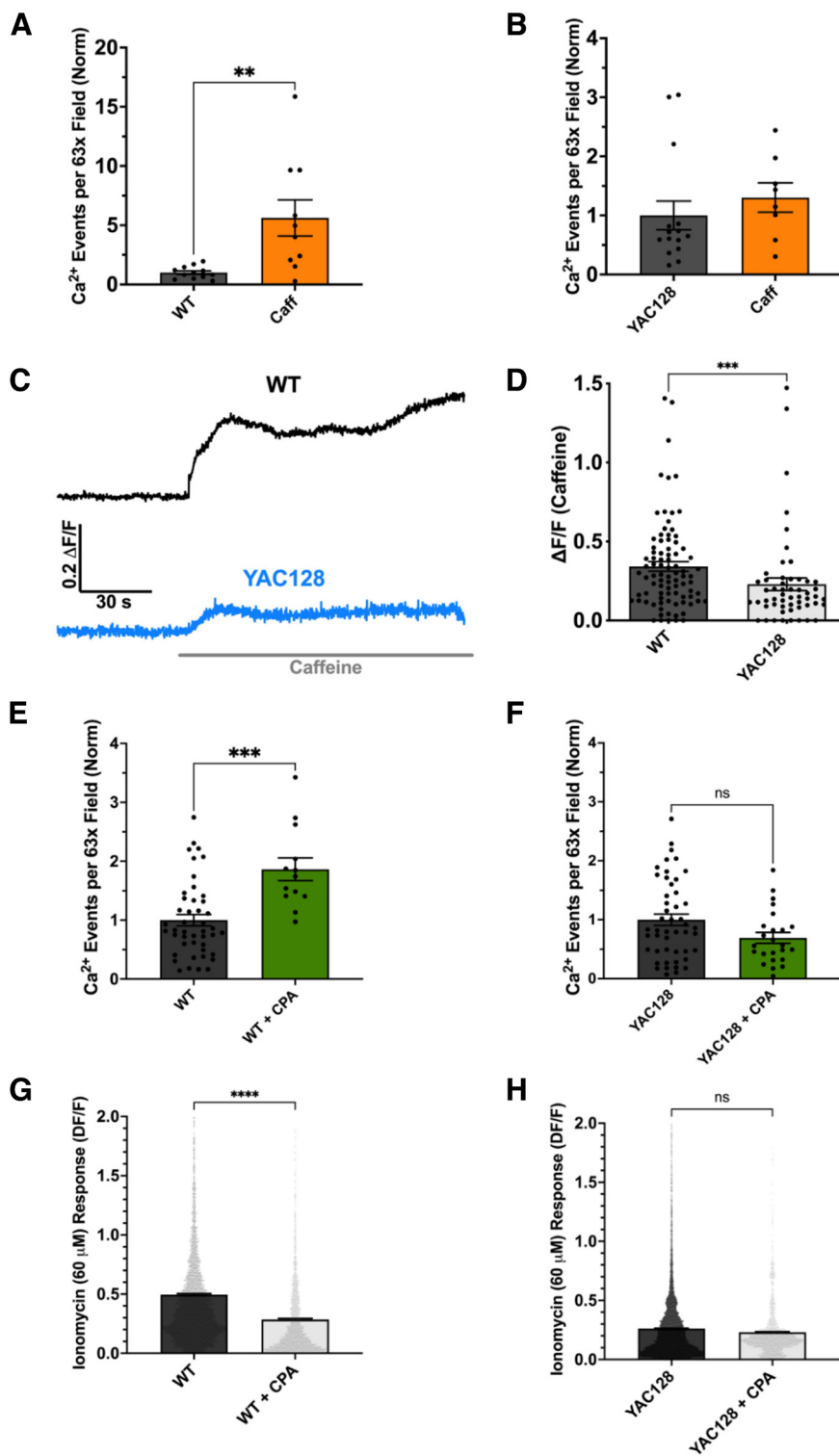


Figure 8. Pharmacologically releasing ER Ca²⁺ increases the frequency of miniature Ca²⁺ events and the resting Ca²⁺ concentration in WT, but not YAC128, cortical axonal boutons. **A, B**, Numbers of miniature axonal Ca²⁺ events detected with the AQUA software in the presence TTX (500 nM) (over 3 min of imaging a 178.6 μm × 113.1 μm 63× objective field) for WT (**A**) and YAC128 (**B**) cortical cultures expressing rSyph-GCaMP6m in the absence or presence of caffeine (1 mM). Numbers of event are normalized to the without caffeine condition for both genotypes. WT axons showed significantly more AP-independent events in the presence of caffeine, than in its absence [5.622 ± 1.524 events/3 min ($n = 12$ fields; 4 cultures)] versus [1.000 ± 0.150 events/3 min ($n = 10$ fields; 5 cultures)], respectively [$t_{(20)} = 3.316$; $p = 0.0034$; Student's unpaired t test]. Numbers of detected YAC128 axonal events were not significantly different in the presence or absence of caffeine [1.303 ± 0.248 events/3 min ($n = 8$ fields; 4 cultures)] versus [1.000 ± 0.224 events/3 min ($n = 15$ fields; 4 cultures)], respectively [$p = 0.2188$ (exact); Mann–Whitney test]. **C**, DF/F time courses from representative WT (top) and YAC128 (bottom) rSyph-GCaMP6m-expressing axonal boutons in the presence of TTX (500 nM) before and immediately following

Together, experiments up to this point suggest that ER Ca²⁺ depletion in YAC128 cultures elevates miniature vesicular glutamate release but may also contribute to reduced AP firing rates, which should ultimately reduce activity-dependent glutamate release.

Evoked glutamate release does not differ between YAC128 and WT cortical-striatal brain slices

We next performed experiments in cortical-striatal *ex vivo* brain slices prepared from 2- to 4-month-old WT and YAC128 mice expressing the fluorescent glutamate

← application of caffeine (1 mM). For this illustration, boutons were selected which did not show miniature Ca²⁺ events. Note the gradual, sustained caffeine (1 mM)-mediated increase in rSyph-GCaMP6m fluorescence, which is of larger magnitude in the WT bouton. **D**, Caffeine responses of WT and YAC128 rSyph-GCaMP6m-expressing boutons in the presence of TTX as illustrated in **C**. Boutons showing miniature Ca²⁺ events (as in Fig. 6) were excluded as the long time course of such events complicated quantification of steady-state increases in DF/F. Caffeine application elicited a significantly greater increase in rSyph-GCaMP6m fluorescence in WT boutons [0.342 ± 0.030 DF/F ($n = 87$ boutons)] compared with YAC128 [0.229 ± 0.039 DF/F ($n = 54$ boutons)] [$p = 0.0004$ (exact); Mann–Whitney test]. **A, B, D**, Five cultures for WT and 5 cultures for YAC128. **E, F**, Numbers of miniature axonal Ca²⁺ events detected with the AQUA software in the presence TTX (500 nM) (as in **A, B**) for WT (**E**) and YAC128 (**F**) cortical cultures expressing rSyph-GCaMP6m (as above) in the absence or presence of CPA (30 μM). Numbers of event are normalized to the without CPA condition for both genotypes. WT axons showed significantly more AP-independent events in the presence of CPA, than in its absence [1.865 ± 0.193 events/3 min ($n = 13$ fields; 3 cultures)] versus [1.000 ± 0.096 events/3 min ($n = 45$ fields; 7 cultures)], respectively [$p = 0.0001$ (exact); Mann–Whitney test]. Numbers of detected YAC128 axonal events were not significantly different in the presence or absence of CPA [0.692 ± 0.093 events/3 min ($n = 24$ fields; 3 cultures)] versus [1.000 ± 0.097 events/3 min ($n = 48$ fields; 6 cultures)], respectively [$p = 0.2188$ (exact); Mann–Whitney test]. **G, H**, Peak DF/F Ca²⁺ responses to ionomycin (60 μM) (not normalized to isosbestic fluorescence) in WT (**G**) and YAC128 (**H**) boutons in TTX, with or without incubation with CPA (30 μM) (>10 min). **G**, Ionomycin (60 μM) responses were significantly reduced in WT boutons following CPA (30 μM) incubation [0.2856 ± 0.0081 DF/F ($n = 2441$ boutons; 3 cultures)] compared with WT boutons without CPA [0.4955 ± 0.0084 DF/F ($n = 5740$ boutons; 6 cultures)] [$p = 0.0016$ (exact); Mann–Whitney test]. Ionomycin (60 μM) responses in YAC128 boutons were smaller than in WT [0.2624 ± 0.0024 DF/F ($n = 19,924$ boutons; 2 cultures)] and were not changed following incubation with CPA (30 μM) [0.2315 ± 0.0050 DF/F ($n = 2020$ boutons; 5 cultures)] [$p = 0.0016$ (exact); Mann–Whitney test]. Analysis was restricted to GCaMP6m-expressing boutons colocalized with mCherry-PSD95-tagged dendritic spines. Ionomycin data for WT and YAC128 boutons in the absence of CPA have been previously shown and compared in Figure 6. *** $p < 0.01$. **** $p < 0.001$. **** $p < 0.0001$.

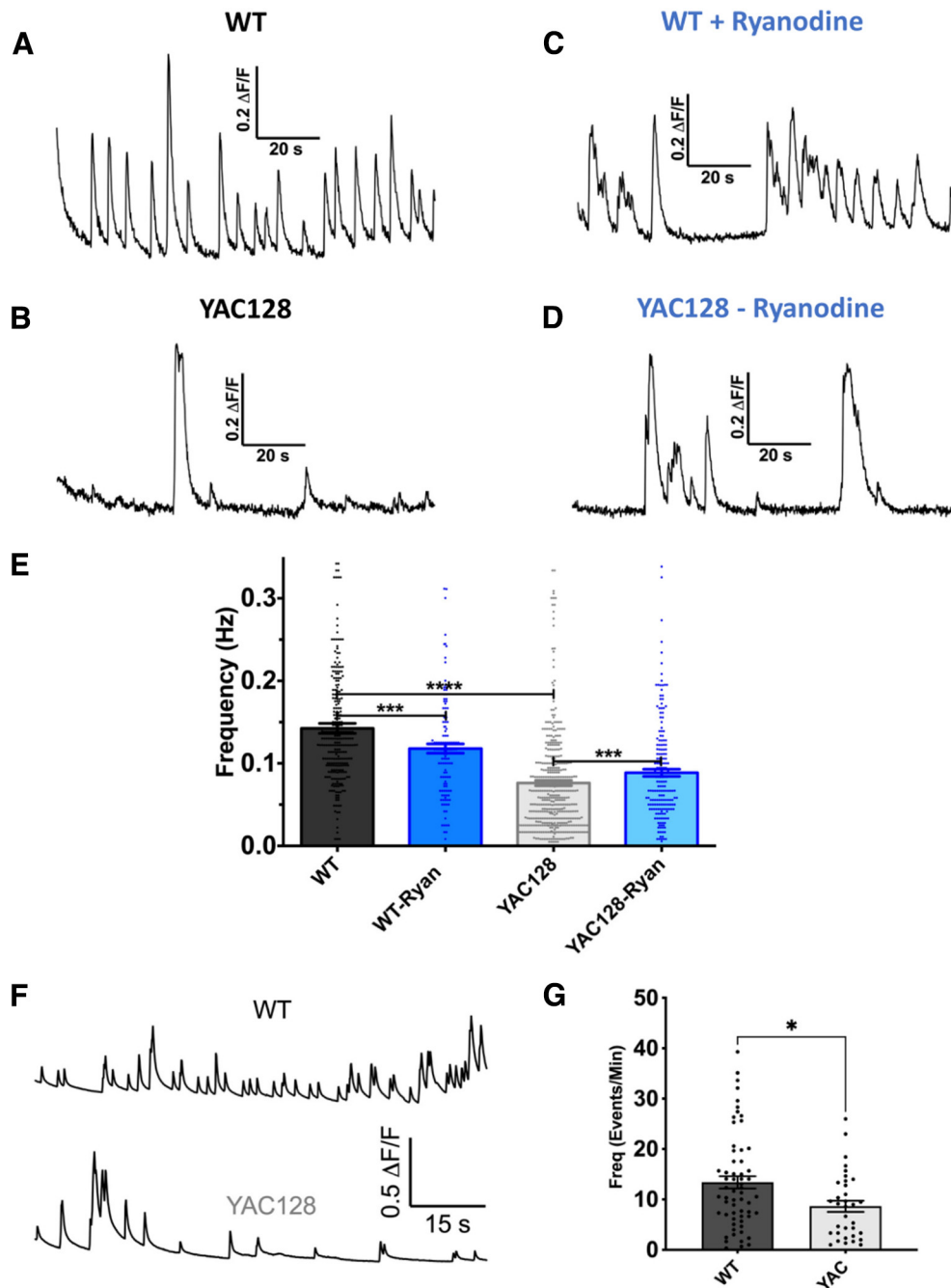


Figure 9. Spontaneous Ca²⁺ transients are reduced in boutons in YAC128 cortical cultures because of decreased AP firing. **A, B**, DF/F time course from a representative WT (**A**) and YAC128 (**B**) rSyph-GCaMP6m-expressing axonal boutons in the absence of TTX. Note the substantially higher spontaneous event frequency in the WT versus YAC128 bouton. **C, D**, DF/F time course from a representative WT (**C**) and YAC128 (**D**) rSyph-GCaMP6m-expressing axonal boutons in the absence of TTX and in the presence of 5 μ M ryanodine. **E**, Mean Ca²⁺ event frequencies of rSyph-GCaMP6m-expressing boutons in the absence of TTX in WT and YAC128 cortical cultures in the presence and absence of ryanodine (5 μ M). Select comparisons were made with the Mann–Whitney test because event widths in all groups failed the D’Agostino–Pearson omnibus normality test. Events were significantly more frequent in WT boutons [0.1424 ± 0.0061 Hz ($n = 272$ boutons; 5 cultures)] than in YAC128 boutons [0.0761 ± 0.0044 Hz ($n = 423$ boutons; 6 cultures)] [$p < 0.0001$ (approximate); Mann–Whitney test]. Events were significantly less frequent in WT boutons with ryanodine (5 μ M) [0.1179 ± 0.0033 Hz ($n = 120$ boutons, 3 cultures)] than without (above) [$p = 0.0038$ (approximate); Mann–Whitney test]. Conversely, event frequencies were significantly more frequent in YAC128 boutons with ryanodine (5 μ M) [0.0886 ± 0.0044 Hz ($n = 189$ boutons, 4 cultures)] than without (above) [$p = 0.0003$ (approximate); Mann–Whitney test]. **F**, Three minute DF/F time courses from the soma of representative WT (top) and YAC128 (bottom) JGCaMP7f-expressing CPNs in the absence of TTX. **G**, Spontaneous somatic CPN Ca²⁺ events were significantly less frequent in YAC128 cortical cultures [8.648 ± 1.114 events/min ($n = 34$ neurons; 3 cultures)] versus WT [13.39 ± 1.217 events/min ($n = 61$ neurons; 4 cultures)] [$p = 0.0169$ (exact); Mann–Whitney test]. * $p < 0.05$. *** $p < 0.001$. **** $p < 0.0001$.

sensor iGluSnFR in striatal neurons (Parsons et al., 2016; Koch et al., 2018). This preparation allowed direct optical measurement of glutamate release in the striatum, independent of postsynaptic neuronal properties. Striatal iGluSnFR signals evoked by stimulating cortical axons of the corpus callosum (Fig. 10A,B) were

significantly, albeit modestly, decreased by ryanodine (5 μ M) in WT, but not YAC128 slices (Fig. 10C,D). These results suggested that evoked glutamate release may be reduced in YAC128 mice by an ongoing release of axonal ER Ca²⁺ stores, which also occludes YAC128 responses to low-dose ryanodine. To directly

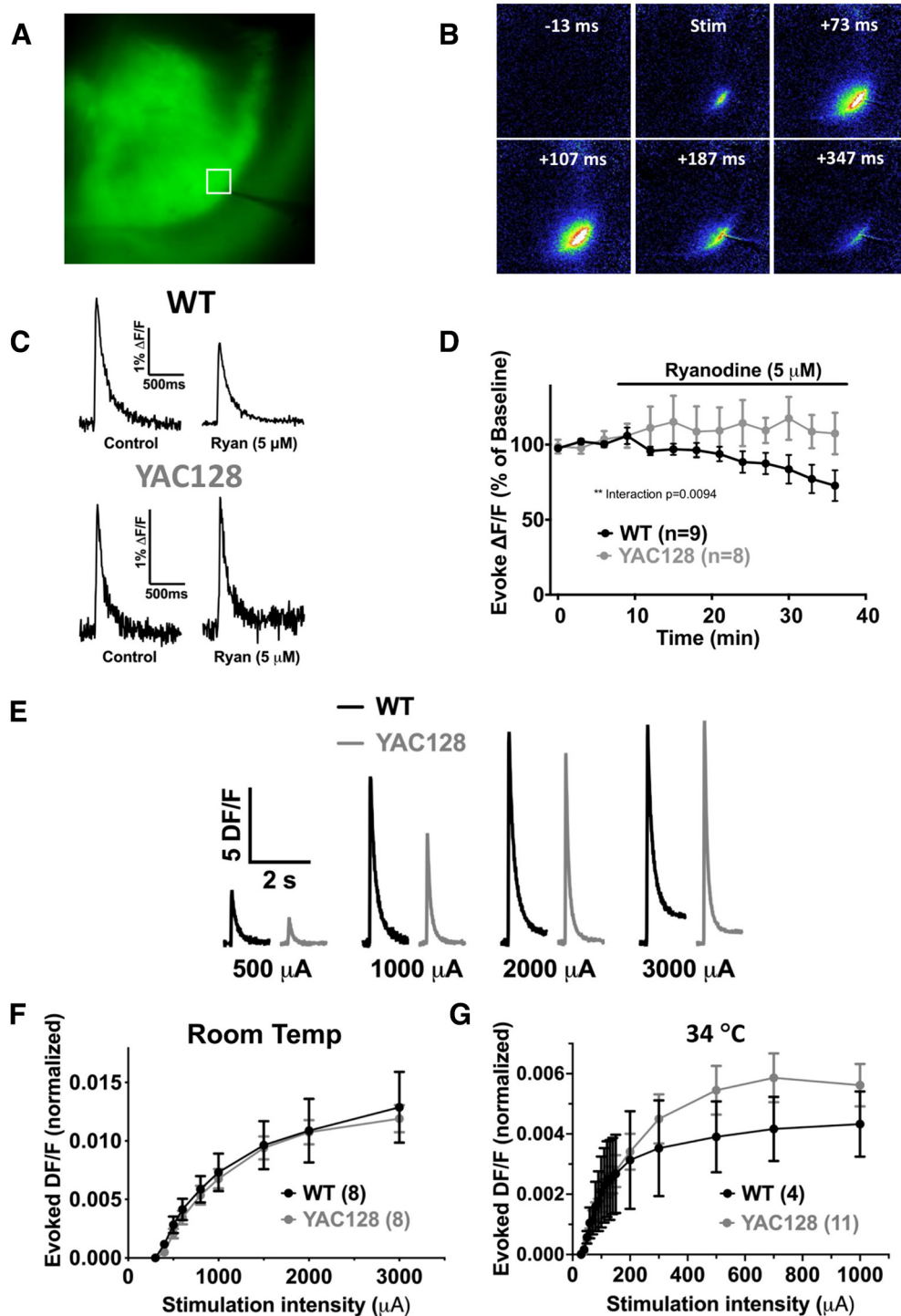


Figure 10. Ryanodine reduces evoked striatal iGluSnR responses in WT, but not YAC128, brain slices, but evoked glutamate release is otherwise similar between genotypes. **A**, Image of raw iGluSnFR fluorescence from a representative WT mouse brain slice with viral-mediated expression of iGluSnFR in its dorsal striatum. Note the square ROI over which evoked spatially averaged DF/F signals were measured, and the tungsten monopolar stimulating electrode placed in the corpus callosum. **B**, A DF/F image montage from the WT brain slice (shown in **A**), illustrating a striatum iGluSnFR response evoked by electrically stimulating cortical axons in the adjacent corpus callosum. **C**, Striatum evoked DF/F iGluSnFR responses from a representative WT (top) and YAC128 (bottom) brain slice before and in the presence of ryanodine (5 μ M). Ryanodine elicits a substantial reduction in the peak WT, but not YAC128, iGluSnFR response. **D**, Peak evoked striatum iGluSnFR responses from WT and YAC128 slices before and during treatment of slices with ryanodine (5 μ M). Responses were measured repeatedly at 3 min intervals and were normalized to the average of each slice's three baseline (before drug) measurements. Ryanodine application decreased the amplitude of the evoked iGluSnFR response in WT ($n = 9$ slices; 9 mice), but not YAC128 ($n = 8$ slices; 8 mice). The effect of ryanodine on WT slices was significantly different from in YAC128 slices, based on a significant time \times genotype interaction ($p = 0.0094$, repeated-measures (time) two-way ANOVA). **E**, Evoked DF/F striatal iGluSnFR responses (as above) to a variety of stimulation intensities (500, 1000, 2000, and 3000 μ A responses shown) conducted at room temperature from a representative WT (black) and YAC128 (gray) slice. Although not shown here, for statistical analysis, DF/F responses were normalized to iGluSnFR fluorescence in the presence of 10 mM glutamate (applied at the end of the experiment under like illumination) to account for potential differences in iGluSnFR expression between slices. **F**, Cortically evoked striatal iGluSnFR responses at room temperature to a variety of stimulation intensities (300, 400, 500, 600, 800, 1000, 1500, 2000, and 3000 μ A), normalized to iGluSnFR fluorescence in the presence of 10 mM glutamate (applied at the end of the experiment under like illumination), from WT (black) and YAC128 (gray) slices. iGluSnFR responses were similar between WT ($n = 8$ slices;

compare evoked cortical glutamate release between genotypes, we next measured striatal-evoked iGluSnFR responses, at a variety of stimulation intensities, then normalized these responses to a near saturating dose of exogenously applied glutamate at the end of the experiment (under like illumination), to account for any differences in iGluSnFR expression between brain slices, animals, and genotypes. However, these experiments revealed similar evoked glutamate responses between genotypes (Fig. 10E,F). de Juan-Sanz et al. (2017) found that axonal ER depletion attenuated evoked glutamate release from hippocampal neurons, but that this effect was only apparent at physiological temperature. As experiments up to this point were performed at room temperature, we also examined striatal-evoked iGluSnFR responses at 34°C. However, we continued to observe no significant difference between WT and YAC128 slices at near physiological temperature (Fig. 10G), suggesting that equivalent cortical AP firing evokes similar glutamate release in the YAC128 and WT striatum at this young age.

Discussion

Presynaptic neurotransmitter release, in concert with postsynaptic signaling, underlies most between-neuron communication and can be divided into AP-dependent and -independent forms. The former requires sodium AP-mediated presynaptic VGCC activation, while the latter persists without neuronal activity. Although miniature neurotransmission is relatively poorly understood, its physiological relevance is increasingly accepted (McKinney et al., 1999; Frank et al., 2006; Sutton et al., 2006). Moreover, miniature release is regulated relatively independently of its AP-dependent counterpart and may use distinct vesicular pools (Sara et al., 2005; Fredj and Burrone, 2009), targeting different postsynaptic receptors (Atasoy et al., 2008).

Altered synaptic signaling, particularly at glutamatergic excitatory synapses, has been reported in HD models (Raymond et al., 2011; Sepers et al., 2018; Tyebji and Hannan, 2017; Cepeda and Levine, 2022) and other neurodegenerative diseases (Wang and Reddy, 2017). Increased SPN extrasynaptic NMDAR expression favors excitotoxic postsynaptic glutamate signaling in HD models (Milnerwood et al., 2010; Dau et al., 2014). Mounting evidence also suggests aberrant glutamate release from cortical afferents in HD; however, the direction of this alteration is disease stage-dependent (Cepeda et al., 2003; Joshi et al., 2009).

The ER, a continuous intracellular membrane-system involved in Ca²⁺ storage and protein synthesis, is found in all neuronal processes, including axons and presynaptic boutons. Increased ER-to-cytosol Ca²⁺ release has been shown in HD models because of enhanced IP3R responsiveness (Tang et al., 2003) and a constituent RyR Ca²⁺ leak (Suzuki et al., 2012). Although previous HD studies have focused on the postsynaptic ER, presynaptic ER Ca²⁺

release is reported to modulate neurotransmission (Llano et al., 2000; Emptage et al., 2001). Our results suggest that mHTT depletes ER Ca²⁺ stores proximal to cortical presynaptic terminals, occluding pharmacological facilitation (by RyR activation) of miniature postsynaptic (glutamate) and presynaptic (Ca²⁺) event frequencies; this underlying ER leak presumably mediates increased basal YAC128 mini glutamate release. However, our results paradoxically suggest that resting cytosolic Ca²⁺ levels are lower in YAC128 than WT boutons, while YAC128 mini axonal Ca²⁺ events were smaller in amplitude and similar in frequency to WT. Furthermore, YAC128 mEPSCs were less sensitive to chelation of intracellular Ca²⁺. The ultimate mechanism by which ER Ca²⁺ dysfunction elevates miniature glutamate release from YAC128 boutons is therefore more complex than simply providing cytosolic Ca²⁺ for vesicular release.

AP-independent cortical glutamate release is selectively elevated in the YAC128 model

No genotype differences were seen in evoked striatal glutamate release in 2- to 4-month-old mice brain slices, despite substantially higher YAC128 SPN mEPSC frequencies, suggesting selective potentiation of miniature glutamate release at this early stage. Others reported altered evoked cortical glutamate release in YAC128 brain slices; however, genotype differences were complex and disease-stage dependent, with early increases followed by reduced release in aged mice (Joshi et al., 2009). Perhaps our experiments were performed during the transition between juvenile and aged phenotypes, obscuring genotype differences. In any case, our results support a dissociation between mHTT's modulation of miniature and evoked glutamate release, consistent with differential regulation of these two forms of neurotransmission. As we have focused exclusively on glutamatergic synapses, future experiments are required to determine whether other neurotransmitter systems are similarly affected.

Elevated YAC128 mEPSC frequencies are mediated by increased glutamate release and not differences in synapse numbers

YAC128 CPNs showed higher mEPSC frequencies at DIV14 and DIV18 (vs WT cultures). Striatal SPNs (which receive substantial excitatory cortical innervation) likewise showed higher mEPSC frequencies in acute brain slices from young YAC128 mice, indicating this phenotype is not an artifact of culture conditions. However, CPN mEPSC frequencies were similar between genotypes by DIV21, consistent with findings of Buren et al. (2016) in a cortical-striatal coculture model, who attributed this to reduced YAC128 SPN total dendritic length (thus, reduced overall synapse numbers). Notably our DIV18-aged cortical cultures, used for mechanistic experiments, showed no genotype differences in CPN synapse density or dendritic morphology, suggesting that differential mEPSC frequencies reflect altered presynaptic release rates. We suspect that increased miniature cortical glutamate release is an early disease feature, most evident in the postsynaptic mEPSC frequency before loss of synaptic connections.

Altered axonal Ca²⁺ waves in YAC128 cultures cannot fully explain differences in miniature glutamate release

RyR agonism, with caffeine or low-dose ryanodine, failed to increase the mEPSC frequency in YAC128 CPNs, despite robustly increasing WT frequencies. This result suggests tonic presynaptic ER Ca²⁺ release chronically elevates mini release in YAC128 cultures, occluding further facilitation. Consistent with this mechanism, caffeine significantly increased the frequency of axonal Ca²⁺

←

5 mice) and YAC128 ($n = 8$ slices; 6 mice) slices across a wide range of stimulation intensities [two-way ANOVA; genotype: $F_{(1, 14)} = 0.1314, p = 0.7224$; stimulation intensity: $F_{(8, 111)} = 58.26, p < 0.0001$; interaction: $F_{(8, 111)} = 0.06491, p = 0.9998$]. **G**, Cortically evoked striatal iGluSnFR responses at 34°C to a variety of stimulation intensities (30, 40, 50, 60, 70, 80, 90, 100, 110, 120, 130, 140, 150, 200, 300, 500, 700, and 1000 μ A), normalized to iGluSnFR fluorescence in the presence of 10 mM glutamate (as in **F**), from WT (black) and YAC128 (gray) slices. iGluSnFR responses were similar between WT ($n = 4$ slices; 4 mice) and YAC128 ($n = 11$ slices; 8 mice) slices across a wide range of stimulation intensities [two-way ANOVA; genotype: $F_{(1,13)} = 0.07220, p = 0.7924$; stimulation intensity: $F_{(17,221)} = 28.32, p < 0.0001$; interaction: $F_{(17, 221)} = 1.263, p = 0.2183$].

waves in WT, but not YAC128 cultures. Similarly, pharmacological inhibition of the ER SERCA pump, known to increase miniature glutamate release in cultured hippocampal neurons (Emptage et al., 2001; Chanaday et al., 2021), increased axonal Ca²⁺ wave frequency and transiently increased cytosolic Ca²⁺ levels in WT, but not YAC128 boutons. Since ionomycin's mechanism of action involves ER Ca²⁺ release and subsequent SOC influx (Morgan and Jacob, 1994; Müller et al., 2013), reduced ionomycin responses in YAC128 boutons also suggest decreased YAC128 axonal ER Ca²⁺ content, as previously reported in YAC128 SPNs (Tang et al., 2003). Interestingly, in 0 extracellular Ca²⁺, WT and YAC128 boutons showed similarly large ionomycin response magnitudes (data not shown), perhaps indicating ER Ca²⁺ depletion in YAC128 boutons requires sufficient extracellular Ca²⁺ to initiate IP₃ and/or ryanodine receptor-mediated Ca²⁺-induced ER Ca²⁺ release with effects of mHTT otherwise masked. Alternatively, CaSRs, which are implicated in mini release, are often Gq-type GPCR coupled, mediating their signaling in part via cytosolic IP₃ release; it is possible this mechanism is upregulated in YAC128 axonal boutons (discussed below).

Amplitudes of axonal Ca²⁺ signals were significantly lower in YAC128 boutons. Likewise, Ca²⁺ waves were more spatially restricted, consistent with reduced YAC128 ER Ca²⁺ content decreasing Ca²⁺ release per individual axonal event. Unexpectedly, miniature axonal wave frequencies were not significantly different between genotypes when measured with the AQuA algorithm, while analysis of mCherry-PSD95 colocalized boutons with our in-house software found significantly lower YAC128 Ca²⁺ event frequencies. However, lower average Ca²⁺ event amplitudes may have caused more events to evade detection in YAC128 cultures, obscuring the expected frequency difference.

Neuronal ER Ca²⁺ waves are predominantly mediated by regenerative IP₃R activity (Nakamura et al., 1999; Larkum et al., 2003; Hagenston et al., 2008); Ca²⁺ released from RyR may modulate these processes (Miyazaki and Ross, 2013), consistent with our data. Spatially restricted, low-amplitude Ca²⁺ puffs from individual IP₃R clusters can induce propagating ER waves but can also remain localized, depending on IP₃ concentrations, cytosolic Ca²⁺ concentrations, and activity of neighboring channel clusters. Increased IP₃R and/or RyR responsiveness in YAC128 cultures might increase axonal wave generation. Conversely, ER Ca²⁺ depletion (because of ongoing release) could also reduce the amplitude of individual Ca²⁺ puffs, such that neighboring receptor cluster activation is impeded and wave generation reduced. Reduced axonal Ca²⁺ event amplitude and area are more consistent with this latter possibility. An increase in the frequency of below-detection-threshold ER Ca²⁺ release events (which would cause ER Ca²⁺ depletion) in concert with reduced complex wave generation, potentially explains our findings. However, based on the reduced sensitivity of YAC128 CPN mEPSCs to BAPTA-AM, any such subdetection-threshold ER release events are unlikely to account for higher YAC128 mEPSC frequencies.

Resting cytosolic Ca²⁺ concentrations are not higher in YAC128 boutons

Surprisingly, basal GCaMP intensity normalized to isosbestic fluorescence was lower in YAC128 boutons, suggesting reduced cytosolic Ca²⁺ concentrations compared with WT. Future experiments using ratiometric Ca²⁺ sensors are needed to definitively test this result. Nonetheless, this refutes the possibility that cytosolic Ca²⁺ concentrations are increased in YAC128 boutons.

It is generally assumed that mHTT elevates cytosolic Ca²⁺ concentrations in vulnerable neuron types. However, conclusions to

this effect have typically been derived from differential responses to pharmacological manipulations, rather than direct cytosolic Ca²⁺ concentration comparisons. One study reported fivefold higher cytosolic Ca²⁺ concentrations in R6/2 mouse SPNs compared with WT, based on ratiometric fura-2 measurements (Hansson et al., 2001); however, neurons were dialyzed with fura-2-containing intracellular solution, presumably altering intracellular signaling and neuronal Ca²⁺ buffering. Additionally, most studies of neuronal Ca²⁺ handling in HD models have focused on striatal SPNs, raising the possibility of differential Ca²⁺ handling in CPNs or specifically in axonal boutons. However, given the exquisite spatial/temporal regulation of Ca²⁺ signaling, it is not surprising that compensatory processes would be engaged to prevent increased spontaneous ER Ca²⁺ release from chronically elevating cytosolic Ca²⁺. We speculate that increased mitochondrial Ca²⁺ uptake or enhanced extrusion via the plasma membrane Ca²⁺ ATPase or Na⁺/Ca²⁺ exchanger underlies such compensation and merits future study.

We found substantial evidence that axonal ER stores are depleted in YAC128 cortical neurons, and that this is associated with increased miniature glutamate release. However, cytosolic Ca²⁺ concentrations were not elevated in YAC128 boutons and YAC128 mini glutamate release was less dependent on intracellular Ca²⁺, suggesting that increased mini glutamate release is not directly mediated by increased ER-to-cytosol Ca²⁺ release or an enhanced SOC response. mEPSC frequencies in YAC128 CPNs were, however, more sensitive to extracellular Ca²⁺, consistent with CaSR upregulation in YAC128 cortical terminals mediating enhanced mini glutamate release. This possibility can be tested in future experiments.

Implications for postsynaptic signaling

Miniature glutamate release can mediate differential postsynaptic signaling (Sutton et al., 2007), and elicits postsynaptic NMDAR-mediated Ca²⁺ influx under physiologically relevant conditions (Espinosa and Kavalali, 2009; Beaulieu-Laroche and Harnett, 2018). In cultures, miniature glutamate-mediated events can become toxic to CPNs following prolonged silencing of neuronal activity with TTX (Fishbein and Segal, 2007). Future studies will be necessary to determine if and how the increased mini glutamate release shown here interacts with the well-described alterations in postsynaptic NMDAR expression in the YAC128 and other HD mouse models, and whether enhanced activity-independent glutamate release contributes to neurodegeneration in HD.

References

- Andreas LC, Burrone J (2015) Spontaneous neurotransmitter release shapes dendritic arbors via long-range activation of NMDA receptors. *Cell Rep* 10:873–882.
- Huntington's Disease Collaborative Research Group (1993) A novel gene containing a trinucleotide repeat that is expanded and unstable on Huntington's disease chromosomes. *Cell* 72:971–983.
- Atasoy D, Ertunc M, Moulder KL, Blackwell J, Chung C, Su J, Kavalali ET (2008) Spontaneous and evoked glutamate release activates two populations of NMDA receptors with limited overlap. *J Neurosci* 28:10151–10166.
- Barnett LM, Hughes TE, Drobizhev M (2017) Deciphering the molecular mechanism responsible for GCaMP6m's Ca²⁺-dependent change in fluorescence. *PLoS One* 12:e0170934.
- Beal MF, Kowall NW, Ellison DW, Mazurek MF, Swartz KJ, Martin JB (1986) Replication of the neurochemical characteristics of Huntington's disease by quinolinic acid. *Nature* 321:168.
- Beaulieu-Laroche L, Harnett MT (2018) Dendritic spines prevent synaptic voltage clamp. *Neuron* 97:75–82.e3.

- Botelho EP, Wang E, Chen JY, Holley S, Andre V, Cepeda C, Levine MS (2014) Differential synaptic and extrasynaptic glutamate-receptor alterations in striatal medium-sized spiny neurons of aged YAC128 Huntington's disease mice. *PLoS Curr* 6:ecurrnts.hd.34957c4f8bd7cb1f5ec47381dfc811c3.
- Buren C, Parsons MP, Smith-Dijk A, Raymond LA (2016) Impaired development of cortico-striatal synaptic connectivity in a cell culture model of Huntington's disease. *Neurobiol Dis* 87:80–90.
- Carter AG, Regehr WG (2002) Quantal events shape cerebellar interneuron firing. *Nat Neurosci* 5:1309–1318.
- Cepeda C, Hurst RS, Calvert CR, Hernández-Echeagaray E, Nguyen OK, Jocoy E, Christian LJ, Ariano MA, Levine MS (2003) Transient and progressive electrophysiological alterations in the corticostriatal pathway in a mouse model of Huntington's disease. *J Neurosci* 23:961–969.
- Cepeda C, Levine MS (2022) Synaptic dysfunction in huntington's disease: Lessons from genetic animal models. *Neuroscientist* 28:20–40.
- Chanaday NL, Nosyreva E, Shin OH, Zhang H, Aklan I, Atasoy D, Bezprozvanny I, Kavalali ET (2021) Presynaptic store-operated Ca²⁺ entry drives excitatory spontaneous neurotransmission and augments endoplasmic reticulum stress. *Neuron* 109:1314–1332.e1315.
- Chen TW, Wardill TJ, Sun Y, Pulver SR, Renninger SL, Baohua A, Schreier ER, Kerr RA, Orger MB, Jayaraman V, Looger LL, Svoboda K, Kim DS (2013) Ultrasensitive fluorescent proteins for imaging neuronal activity. *Nature* 499:295–300.
- de Juan-Sanz J, Holt GT, Schreier ER, de Juan F, Kim DS, Ryan TA (2017) Axonal endoplasmic reticulum Ca²⁺ content controls release probability in CNS nerve terminals. *Neuron* 93:867–881.e6.
- Dau A, Gladding CM, Sepers MD, Raymond LA (2014) Chronic blockade of extrasynaptic NMDA receptors ameliorates synaptic dysfunction and pro-death signaling in Huntington disease transgenic mice. *Neurobiol Dis* 62:533–542.
- Emptage NJ, Reid CA, Fine A (2001) Calcium stores in hippocampal synaptic boutons mediate short-term plasticity, store-operated Ca²⁺ entry, and spontaneous transmitter release. *Neuron* 29:197–208.
- Ermolyuk YS, Alder FG, Surges R, Pavlov IY, Timofeeva Y, Kullmann DM, Volynski KE (2013) Differential triggering of spontaneous glutamate release by P/Q-, N- and R-type Ca²⁺ channels. *Nat Neurosci* 16:1754–1763.
- Espinosa F, Kavalali ET (2009) NMDA receptor activation by spontaneous glutamatergic neurotransmission. *J Neurophysiol* 101:2290–2296.
- Fan MM, Fernandes HB, Zhang LY, Hayden MR, Raymond LA (2007) Altered NMDA receptor trafficking in a yeast artificial chromosome transgenic mouse model of Huntington's disease. *J Neurosci* 27:3768–3779.
- Fishbein I, Segal M (2007) Miniature synaptic currents become neurotoxic to chronically silenced neurons. *Cereb Cortex* 17:1292–1306.
- Frank CA, Kennedy MJ, Goold CP, Marek KW, Davis GW (2006) Mechanisms underlying the rapid induction and sustained expression of synaptic homeostasis. *Neuron* 52:663–677.
- Fredj NB, Burrone J (2009) A resting pool of vesicles is responsible for spontaneous vesicle fusion at the synapse. *Nat Neurosci* 12:751–758.
- Graveland GA, Williams RS, DiFiglia M (1985) Evidence for degenerative and regenerative changes in neostriatal spiny neurons in Huntington's disease. *Science* 227:770–773.
- Gross GG, Junge JA, Mora RJ, Kwon HB, Olson CA, Takahashi TT, Liman ER, Ellis-Davies GC, McGee AW, Sabatini BL, Roberts RW, Arnold DB (2013) Recombinant probes for visualizing endogenous synaptic proteins in living neurons. *Neuron* 78:971–985.
- Hagenston AM, Fitzpatrick JS, Yeckel MF (2008) mGluR-mediated calcium waves that invade the soma regulate firing in layer V medial prefrontal cortical pyramidal neurons. *Cereb Cortex* 18:407–423.
- Hansson O, Guatteo E, Mercuri NB, Bernardi G, Li XJ, Castilho RF, Brundin P (2001) Resistance to NMDA toxicity correlates with appearance of nuclear inclusions, behavioural deficits and changes in calcium homeostasis in mice transgenic for exon 1 of the huntington gene. *Eur J Neurosci* 14:1492–1504.
- Hantraye P, Riche D, Maziere M, Isacson O (1990) A primate model of Huntington's disease: behavioral and anatomical studies of unilateral excitotoxic lesions of the caudate-putamen in the baboon. *Exp Neurol* 108:91–104.
- Hardingham GE, Bading H (2010) Synaptic versus extrasynaptic NMDA receptor signalling: implications for neurodegenerative disorders. *Nat Rev Neurosci* 11:682–696.
- Joshi PR, Wu NP, André VM, Cummings DM, Cepeda C, Joyce JA, Carroll JB, Leavitt BR, Hayden MR, Levine MS, Bamford NS (2009) Age-dependent alterations of corticostriatal activity in the YAC128 mouse model of Huntington disease. *J Neurosci* 29:2414–2427.
- Koch ET, Woodard CL, Raymond LA (2018) Direct assessment of presynaptic modulation of cortico-striatal glutamate release in a Huntington's disease mouse model. *Neurophysiol* 120:3077–3084.
- Kovalenko M, Milnerwood A, Giordano J, St Claire J, Guide JR, Stromberg M, Gillis T, Sapp E, DiFiglia M, MacDonald ME, Carroll JB, Lee JM, Tappan S, Raymond L, Wheeler VC (2018) HttQ111/+ Huntington's disease knock-in mice exhibit brain region-specific morphological changes and synaptic dysfunction. *J Huntingtons Dis* 7:17–33.
- Larkum ME, Watanabe S, Nakamura T, Lasser-Ross N, Ross WN (2003) Synaptically activated Ca²⁺ waves in layer 2/3 and layer 5 rat neocortical pyramidal neurons. *J Physiol* 549:471–488.
- Li H, Wyman T, Yu ZX, Li SH, Li XJ (2003) Abnormal association of mutant huntingtin with synaptic vesicles inhibits glutamate release. *Hum Mol Genet* 12:2021–2030.
- Lindhout FW, Cao Y, Kevenaar JT, Bodzeta A, Stucchi R, Boumpoutsari MM, Katrukha EA, Altelaar M, MacGillivray HD, Hoogenraad CC (2019) VAP-SCRNI interaction regulates dynamic endoplasmic reticulum remodeling and presynaptic function. *EMBO J* 38:e101345.
- Llano I, González J, Caputo C, Lai FA, Blayney LM, Tan YP, Marty A (2000) Presynaptic calcium stores underlie large-amplitude miniature IPSCs and spontaneous calcium transients. *Nat Neurosci* 3:1256–1265.
- Marvin JS, Borghuis BG, Tian L, Cichon J, Harnett MT, Akerboom J, Gordus A, Renninger SL, Chen TW, Bargmann CI, Orger MB, Schreier ER, Demb JB, Gan WB, Hires SA, Looger LL (2013) An optimized fluorescent probe for visualizing glutamate neurotransmission. *Nat Methods* 10:162–170.
- McKinney RA, Capogna M, Dürr R, Gähwiler BH, Thompson SM (1999) Miniature synaptic events maintain dendritic spines via AMPA receptor activation. *Nat Neurosci* 2:44–49.
- Meissner G (2017) The structural basis of ryanodine receptor ion channel function. *J Gen Physiol* 149:1065–1089.
- Milnerwood AJ, Gladding CM, Pouladi MA, Kaufman AM, Hines RM, Boyd JD, Ko RW, Vasuta OC, Graham RK, Hayden MR, Murphy TH, Raymond LA (2010) Early increase in extrasynaptic NMDA receptor signaling and expression contributes to phenotype onset in Huntington's disease mice. *Neuron* 65:178–190.
- Milnerwood AJ, Kaufman AM, Sepers MD, Gladding CM, Zhang L, Wang L, Fan J, Coquinco A, Qiao JY, Lee H, Wang YT, Cynader M, Raymond LA (2012) Mitigation of augmented extrasynaptic NMDAR signaling and apoptosis in cortico-striatal co-cultures from Huntington's disease mice. *Neurobiol Dis* 48:40–51.
- Miyazaki K, Ross WN (2013) Ca²⁺ sparks and puffs are generated and interact in rat hippocampal CA1 pyramidal neuron dendrites. *J Neurosci* 33:17777–17788.
- Morgan AJ, Jacob R (1994) Ionomycin enhances Ca²⁺ influx by stimulating store-regulated cation entry and not by a direct action at the plasma membrane. *Biochem J* 300:665–672.
- Müller MS, Obel LF, Waagepetersen HS, Schousboe A, Bak LK (2013) Complex actions of ionomycin in cultured cerebellar astrocytes affecting both calcium-induced calcium release and store-operated calcium entry. *Neurochem Res* 38:1260–1265.
- Nakamura T, Barbara JG, Nakamura K, Ross WN (1999) Synergistic release of Ca²⁺ from IP₃-sensitive stores evoked by synaptic activation of mGluRs paired with backpropagating action potentials. *Neuron* 24:727–737.
- Nelson CJ, Duckney P, Hawkins TJ, Deeks MJ, Laissue PP, Hussey PJ, Obara B (2015) Blobs and curves: object-based colocalisation for plant cells. *Funct Plant Biol* 42:471–485.
- Parsons MP, Vanni MP, Woodard CL, Kang R, Murphy TH, Raymond LA (2016) Real-time imaging of glutamate clearance reveals normal striatal uptake in Huntington disease mouse models. *Nat Commun* 7:11251.
- Plotkin JL, Day M, Peterson JD, Xie Z, Kress GJ, Rafalovich I, Kondapalli J, Gertler TS, Flajolet M, Greengard P, Stavarache M, Kaplitt MG, Rosinski J, Chan CS, Surmeier DJ (2014) Impaired TrkB receptor signaling underlies corticostriatal dysfunction in Huntington's disease. *Neuron* 83:178–188.
- Raymond LA (2017) Striatal synaptic dysfunction and altered calcium regulation in Huntington disease. *BBRC* 483:1051–1062.

- Raymond LA, André VM, Cepeda C, Gladding CM, Milnerwood AJ, Levine MS (2011) Pathophysiology of Huntington's disease: time-dependent alterations in synaptic and receptor function. *Neuroscience* 198:252–273.
- Ross WN (2012) Understanding calcium waves and sparks in central neurons. *Nat Rev Neurosci* 13:157–168.
- Sara Y, Virmani T, Deák F, Liu X, Kavalali ET (2005) An isolated pool of vesicles recycles at rest and drives spontaneous neurotransmission. *Neuron* 45:563–573.
- Sepers MD, Smith-Dijk A, LeDue J, Kolodziejczyk K, Mackie K, Raymond LA (2018) Endocannabinoid-specific impairment in synaptic plasticity in striatum of huntington's disease mouse model. *J Neurosci* 38:544–554.
- Sharma G, Vijayaraghavan S (2003) Modulation of presynaptic store calcium induces release of glutamate and postsynaptic firing. *Neuron* 38:929–939.
- Slow EJ, van Raamsdonk J, Rogers D, Coleman SH, Graham RK, Deng Y, Oh R, Bissada N, Hossain SM, Yang YZ, Li XJ, Simpson EM, Gutekunst CA, Leavitt BR, Hayden MR (2003) Selective striatal neuronal loss in a YAC128 mouse model of Huntington disease. *Hum Mol Genet* 12:1555–1567.
- Smith-Dijk AI, Nassrallah WB, Zhang LY, Geva M, Hayden MR, Raymond LA (2019) Impairment and restoration of homeostatic plasticity in cultured cortical neurons from a mouse model of Huntington disease. *Front Cell Neurosci* 13:209.
- Sutton MA, Ito HT, Cressy P, Kempf C, Woo JC, Schuman EM (2006) Miniature neurotransmission stabilizes synaptic function via tonic suppression of local dendritic protein synthesis. *Cell* 125:785–799.
- Sutton MA, Taylor AM, Ito HT, Pham A, Schuman EM (2007) Postsynaptic decoding of neural activity: eEF2 as a biochemical sensor coupling miniature synaptic transmission to local protein synthesis. *Neuron* 55:648–661.
- Suzuki M, Nagai Y, Wada K, Koike T (2012) Calcium leak through ryanodine receptor is involved in neuronal death induced by mutant huntingtin. *Biochem Biophys Res Commun* 429:18–23.
- Tang TS, Guo C, Wang H, Chen X, Bezprozvanny I (2009) Neuroprotective effects of inositol 1,4,5-trisphosphate receptor C-terminal fragment in a Huntington's disease mouse model. *J Neurosci* 29:1257–1266.
- Tang TS, Tu H, Chan EY, Maximov A, Wang Z, Wellington CL, Hayden MR, Bezprozvanny I (2003) Huntingtin and huntingtin-associated protein 1 influence neuronal calcium signaling mediated by inositol-(1,4,5) triphosphate receptor type 1. *Neuron* 39:227–239.
- Tyebji S, Hannan AJ (2017) Synaptopathic mechanisms of neurodegeneration and dementia: Insights from Huntington's disease. *Prog Neurobiol* 153:18–45.
- Vonsattel JP, Myers RH, Stevens TJ, Ferrante RJ, Bird ED, Richardson EP (1985) Neuropathological classification of Huntington's disease. *J Neuropathol Exp Neurol* 44:559–577.
- Vyleta NP, Smith SM (2011) Spontaneous glutamate release is independent of calcium influx and tonically activated by the calcium-sensing receptor. *J Neurosci* 31:4593–4606.
- Wang Y, DelRosso NV, Vaidyanathan TV, Cahill MK, Reitman ME, Pittolo S, Mi X, Yu G, Poskanzer KE (2019) Accurate quantification of astrocyte and neurotransmitter fluorescence dynamics for single-cell and population-level physiology. *Nat Neurosci* 22:1936–1944.
- Wang R, Reddy PH (2017) Role of glutamate and NMDA receptors in Alzheimer's disease. *J Alzheimers Dis* 57:1041–1048.
- Xu J, Pang ZP, Shin OH, Südhof TC (2009) Synaptotagmin-1 functions as a Ca²⁺ sensor for spontaneous release. *Nat Neurosci* 12:759–766.
- Yamasaki M, Hashimoto K, Kano M (2006) Miniature synaptic events elicited by presynaptic Ca²⁺ rise are selectively suppressed by cannabinoid receptor activation in cerebellar Purkinje cells. *J Neurosci* 26:86–95.
- Zeron MM, Hansson O, Chen N, Wellington CL, Leavitt BR, Brundin P, Hayden MR, Raymond LA (2002) Increased sensitivity to N-methyl-D-aspartate receptor-mediated excitotoxicity in a mouse model of Huntington's disease. *Neuron* 33:849–860.